2020

Dynamic Modeling and Simulation of a Power Plant Steam Condenser on the Siemens SPPA-T3000 Platform

Mohammad Odeh
University of Central Florida

DYNAMIC MODELING AND SIMULATION OF A POWER PLANT STEAM CONDENSER ON THE SIEMENS SPPA-T3000 PLATFORM

by

MOHAMMAD ODEH
B.S. University of Central Florida, 2018

A thesis submitted in partial fulfillment of the requirements
for the degree of Master of Science
in the Department of Mechanical and Aerospace Engineering
in the College of Engineering and Computer Science
at the University of Central Florida
Orlando, Florida

Spring Term
2020

ABSTRACT

With rapidly increasing computational power, modeling and simulation of complex systems is becoming the norm for evaluating and predicting performance. This research focuses on modeling and simulating thermodynamic behavior of condensers within Combined Cycle Power Plants. This is particularly useful for power generation companies as this allows a wide range of operating conditions to be simulated and characterized without risking damage or the need to shut down the power plant, all of which results in losing revenue. Moreover, being able to observe the thermodynamic evolution of the system provides insight into efficiency and response to perturbation.

To this end, a dynamic model of a condenser is developed using Siemens Power Plant Automation T3000 (SPPA-T3000), Siemens' proprietary plant monitoring software. The model is simulated using the geometry and specifications of a reference condenser provided by Siemens Energy Inc., along with operating conditions and multiple data sets for model validation. The condenser is modeled using lumped control volumes coupled by heat and mass transfer. Based on extensive literature survey, the model incorporates accurate and time-varying formulations of derived thermodynamic quantities and other heat transfer and fluid flow related coefficients, such as heat capacities, dynamic viscosity, thermal conductivity, and heat transfer coefficients, ensuring the simulation's validity over a wide range of operating conditions.

The model is capable of predicting and simulating both phase changes from steam to liquid water (condensation) and liquid water to steam (evaporation). The latter occurs, over short durations, when the condensate experiences low pressure above it. A switching mechanism is implemented to transition between different modes of operation and model the process of temperature change and mass transfer in each mode. The resulting simulation values for temperature and pressure agree with those provided by Siemens Energy Inc. for different operating conditions.

I would like to dedicate this work to my family. I would not be where I am today were it not for their sacrifices. To each and everyone, thank you.

ACKNOWLEDGMENTS

First and foremost, I would like to thank my advisor Dr. Tuhin Das for his continuous support, thought provoking discussions, and patience while mentoring me. I am very thankful for the opportunity that he has provided by involving me in the research at his lab as it was always challenging me to improve and grow as an engineer. I would also like to extend my thanks to Jonathan McConnell, my lab colleague, for guiding me through SPPA-T3000 and answering the many questions I had.

In addition, I would like to thank Andres Caesar, James Hoy, and Prithvi Veeravalli, our lab's contacts at Siemens Energy Inc. This project would not have come to fruition were it not for their support and help. The data they provided me was essential to this project.

Last but not least, I would like thank the committee members Dr. Ranajay Ghosh and Dr. Tian Tian for taking interest in my work and generously offering their time throughout the preparation and review of this document as well as the thesis defense.

TABLE OF CONTENTS

LIST OF FIGURES ix

LIST OF TABLES xi

LIST OF SYMBOLS xii

CHAPTER 1: INTRODUCTION 1

1.1 Rationale 1

1.2 Literature Review 1

1.3 Objective 4

1.4 Method 5

CHAPTER 2: BACKGROUND 7

2.1 Rankine Cycle 7

2.2 Steam Condenser 8

2.3 SPPA-T3000 9

CHAPTER 3: CONDENSER THERMODYNAMICS AND MODELING 13

3.1 Metal Control Volume ($C\forall_{met}$) 13

3.1.1 Mathematical Formulation 14

3.2 Vapor Control Volume ($C\not{V}_{vap}$) 19

3.2.1 Mathematical Formulation 21

3.2.2 Convective Heat Transfer Coefficient Estimation 23

3.2.3 Superheat Correction Factor 27

3.2.4 Temperature Evolution and Mass Transfer 30

3.3 Liquid Control Volume ($C\not{V}_{liq}$) 35

3.3.1 Mathematical Formulation 37

3.3.2 Temperature Evolution and Mass Transfer 38

3.3.3 Flash Steam 40

CHAPTER 4: MODEL VALIDATION 45

4.1 Condenser Operation 45

4.2 Steady-State Values 47

4.3 Simulations 49

4.4 Response to Perturbation 52

CHAPTER 5: CONCLUSION AND FUTURE WORK 54

5.1 Overview 54

5.2 Future Research 55

5.2.1 Improvements 55

5.2.2 Superheated Steam HTC Prediction 55

5.2.3 Attemperation 56

5.2.4 Implementation with HRSG, Steam Turbine, and Pump Models 56

APPENDIX : SPPA-T3000 MODEL 57

LIST OF REFERENCES 59

LIST OF FIGURES

2.1 T-s diagram 8

2.2 Shell-and-Tube Heat Exchanger 9

2.3 Sample collection of function blocks 11

2.4 Embedded diagram 11

2.5 Real-time signal input/output display 12

3.1 Metal Control Volume ($C\forall_{met}$) 13

3.2 Metal Control Volume ($C\forall_{met}$) in SPPA-T3000. Top view (left) and 1st level embedded diagram (right) 19

3.3 Modes of condensation. Film condensation (left) and dropwise condensation (right) 20

3.4 Experimental data vs. Butterworth [23] model (adapted from Rose [28]) . . . 26

3.5 $c_{p,vap}$ and $c_{\forall,vap}$ computation logic 30

3.6 Close-up of T-s diagram – cooling mode 31

3.7 Condensing mode. Initial oscillatory behavior (left) and steady-state operation (right) 32

3.8 Switching logic schematic 33

3.9 Switching logic in SPPA-T3000 36

3.10 Closed 2 partitions system 41

3.11 Liquid Control Volume ($C\forall_{liq}$) in SPPA-T3000 44

4.1 Flash steam generation 46

4.2 Condensation rate. Case 1 (left) and case 2 (right) 47

4.3 Temperature evolution. Case 1 (left) and case 2 (right) 48

4.4 Pressure evolution. Case 1 (left) and case 2 (right) 49

4.5 Dynamic response 52

.1 Model in SPPA-T3000 58

LIST OF TABLES

3.1 Coolant carrying pipes ($C\not{V}_{met}$) specifications 14

3.2 Vapor space ($C\not{V}_{vap}$) specifications 20

3.3 Coefficients of regression polynomial for $E\,(T)$ and $F\,(T)$ 29

3.4 Condensate liquid ($C\not{V}_{liq}$) specifications 36

3.5 Density coefficients for eq. (3.74) 44

4.1 Comparison of model output vs. Siemens' data at steady-state operation . . . 51

LIST OF SYMBOLS

Physical Constants

π	Ratio of a circle's circumference to its diameter	3.14159	$-$
g	Gravitational acceleration	9.80665	$m\ s^{-2}$
R_{vap}	Vapor (steam) gas constant	461.520	$J\ kg^{-1}\ K^{-1}$

Symbols

χ	Steam quality	$\%$
$\dot{m}_{V2L}$	Time rate of mass transfer - vapor to liquid	$kg\ s^{-1}$
$\dot{Q}_{met \to cw}$	Time rate of heat transfer - metal to coolant	$J\ s^{-1}$
$\dot{Q}_{vap \to met}$	Time rate of heat transfer - vapor to metal	$J\ s^{-1}$
$\dot{T}$	Time rate change of temperature	$K\ s^{-1}$
$\not{v}_f$	Specific volume - fluid	$m^3\ kg^{-1}$
$\not{v}_g$	Specific volume - gas	$m^3\ kg^{-1}$
$\not{V}$	Volume	m^3
μ	Dynamic viscocity	$kg\ m^{-1}\ s^{-1}$
ρ	Density	$kg\ m^{-3}$
ε	Deadband value	$-$
$\widetilde{Re}$	Two-phase Reynold's number	$-$

ζ	Superheat correction factor	$-$
c	Specific heat	$J\ kg^{-1}\ K^{-1}$
c_p	Specific heat - constant pressure	$J\ kg^{-1}\ K^{-1}$
c_v	Specific heat - constant volume	$J\ kg^{-1}\ K^{-1}$
D_{in}	Inner diameter	m
D_{out}	Outer diameter	m
H	Convective heat transfer coefficient	$J\ s^{-1}\ m^{-2}\ K^{-1}$
h_{fg}	Latent heat of vaporization	$J\ kg^{-1}$
k	Conductive heat transfer coefficient	$J\ s^{-1}\ m^{-1}\ K^{-1}$
L_c	Characteristic length	m
L_{pipe}	Length of pipe	m
m	Mass	kg
N_{pipe}	Number of pipes	$-$
Nu	Nusselt's number	$-$
q''	Heat flux	$J\ s^{-1}\ m^{-2}$
R_{in}	Inner radius	m
R_{out}	Outer radius	m
T	Thermodynamic temperature	K
v_f	Steam approach velocity	$m\ s^{-1}$

Abbreviations

AFXR	Analog Transfer Switch
AIChE	American Institute of Chemical Engineers
ASME	American Society of Mechanical Engineers
C~~V~~	Control Volume
CCPP	Combined Cycle Power Plnat
DCS	Distributed Control System
DIPPR	Design Institute for Physical Properties
EPRI	Electric Power Research Institute
IAPWS	International Association for the Properties of Water and Steam
PID	Proportional-Integral-Derivative
RHS	Right Hand Side
VPL	Visual Programming Language

Subscripts

cw	Cooling water
dp	Dew point
f	Fluid
g	Gas
HX	Heat exchanger

$L2V$	Liquid to vapor
liq	Liquid
met	Metal
sat	Saturation
sh	Superheat
tr	Triple point
$V2L$	Vapor to liquid
vap	Vapor
vp	Vacuum pump

CHAPTER 1: INTRODUCTION

1.1 Rationale

As the population of earth grows, the demand for energy is ever increasing. The Research and Development (R&D) sector is always looking for ways to improve current energy production technologies. With the advent of computers and the exponential growth in computational power, the ability to construct and simulate complex models has become more feasible than ever. This advancement allows the R&D sector to look into the transient and steady-state behavior of dynamic systems for evaluation purposes. When it comes to power plants, such simulations are beneficial to observe the thermodynamic evolution of constituent power plant modules in order to have a better insight as to how efficiency can be maximized. Furthermore, having a dynamic model of a power plant permits power generation companies to simulate various operation conditions/scenarios prior to implementation without risk of damaging equipment, in addition to being able to see how the power plant responds to perturbations (i.e a sudden increase/decrease in required power generation). Having knowledge about the power plant's dynamics allows the operator to manage the power plant operation and regulation. Aside from power generation companies, humanity as whole will also reap the benefits of such models as being able to efficiently generate sufficient power on-demand while reducing waste energy will help combat climate change.

1.2 Literature Review

Nowadays, more than ever, it is very important for power plant operators to satisfy high standards with regards to economy and environment. The rejection of excess heat into the environment throughout the past years has been adversely affecting life on earth as can be observed from recent

events: an upward trend in increasing positive temperature anomaly [1], deteriorating state of the Great Barrier Reef [2], the untamed wild bush fires in Australia [3], and the decline in global glacier content [4], to name a few. Thus, accurate predictions of power plant performance during start-up and steady-state operation is vital to ensure maximum performance is achieved, and hence, the least amount of waste heat is rejected into the environment. The condenser, a complex shell-and-tube heat exchanger, is one the most vital auxiliary systems in a CCPP as it affects the safety, economic, and environmental operation of the entire power plant [5] . On average, a CCPP has an efficiency of 60% [6], that is, 40% of the heat generated gets dissipated into the environment either through the stack or a condenser.

Numerous studies and publications have been released in the past two decades in regards to the mathematical modeling of steam condensers for design optimization and/or the prediction of operational performance as such knowledge can lead to reduction in operation costs, generated electricity price, and waste heat rejection. In previous years the optimization of condensers was done using a trial-and-error approach based on collected data [7]. However, without detailed insight into the interplay between heat and mass transfer that occurs within the condenser, design optimization is limited as well as information regarding the dynamic response of the condenser. Moreover, conducting experiments on various physical designs can prove laborious and financially expensive [8]. Therefore, the appeal of a numerical condenser model stems from the fact that previously mentioned limitations can be mitigated.

In a research paper published by Zhang [9], a numerical model for a large power plant condenser was proposed to predict performance. However, the model assumed a one-phase flow inside the condenser; condensate that formed on the tube bundles was instantaneously neglected, which led to the shearing effects between the two phases not being taken into consideration. Moreover, a study performed by Roy et al. [10] aimed at modeling a power plant steam condenser by discretizing the interior into subdomains and applying the steady-state, steady-flow conservation equations. Their

model was able to replicate the steady-state values of temperature and pressure to a negligible error. Nonetheless, the model was not capable of predicting the transient-state of the condenser due to the inherent limitation of the steady-state conservation equations. In addition, discretizing the interior imposed longer computational times and resources. Furthermore, Yi Cao at the Cranfield University, UK [11] developed a dynamic model of a steam condenser based on energy balance, however, the model assumes that the inlet steam and outlet condensate are always at saturation pressure and temperature. Hence, heat transfer calculations are greatly reduced to simply being the product of the steam mass flowrate into the condenser and the latent heat of vaporization, both of which are readily known variables. This assumption, even though it reduces computational burden, doesn't provide any additional insight as to how the overall system responds to perturbations or even bypass cases where the inlet steam is not always under saturation conditions. In another report published by Bourdouxhe et al. [12], a simplistic model of a heat exchanger for refrigeration systems was developed. The authors considered the co-existence of three refrigerant phases: gaseous at the condenser inlet, two-phase state within the interior, and liquid at the outlet. For sake of simplicity and first order approximations, the authors opted to lump all three zones into one control volume ($C\cancel{V}$) consisting of the two-phase flow and only computing one heat transfer coefficient in the process. This over simplification severely hinders the model's ability to accurately predict the condenser's performance, and hence, such simplistic models are not suitable for power plant operation simulations, where high levels of accuracy and precision are required. A better approach would account for all three zones, adding two more degrees of freedom, which in turn gives better insight as to how the different physical states impact the condenser performance.

Other research has been conducted by Nikitin et al. [13] regarding dynamic numerical modeling of steam condensers, however, even though the model showed good agreement between empirical and analytical results, the empirical data was obtained from lab experiments and not from an operational unit at a power plant. In addition, the research was aimed towards providing a proof-of-

concept for heat transfer in a steam condenser by liquid carbon dioxide (CO_2) boiling, hence, more attention to detail was given to the thermodynamics and heat transfer properties of the CO_2 phase change throughout the cycle. Another dynamic model of a shell-and-tube condenser was developed by Llopis et al. [14]. In their published article, they provide a mathematical model based on mass conservation, energy conservation, and heat transfer fundamentals to predict the the system's response to perturbations. Still, the model provided was only concerned with the overall process of heat exchange between the steam and coolant and the change in enthalpy and did not give any details regarding the evolution of the intensive properties of the system, such as the change of temperature, pressure, specific heat, etc. of any of the $C\forall$'s. Lastly, in a study published by Cuevas et al. [15], a three-zone condenser model was developed. The model took into account the superheat that might be present in the incoming steam at the condenser's inlet, the co-existence of two-phases during condensation, and the presence of the condensate in the condenser's hotwell. However, the model was not capable of predicting transients and was not able to handle perturbations, thus, not providing any extra information regarding the modeled condenser's dynamics.

None of the previous research referenced within the body of the document attempted validating a dynamic, real-time, two-phase flow, numerical model of a power plant steam condenser against data collected from an operational CCPP, leaving an open gap in the scientific community. The research presented in this document aims at filling the gap and to layout a foundation for such a model that is to be used for performance prediction and evaluation.

1.3 Objective

The objective of this research is to develop and validate a robust and dynamic model of a condenser unit used in a Combined Cycle Power Plant (CCPP) in real-time. The condenser is modeled using first-principle thermodynamic theory and a lumped parameter formulation. The use of a physical-

based model, as opposed to a statistical model, enables us to better approximate the behavior of the system as all the inputs are accounted for. Bearing in mind that the system needs to run in real-time, the use of a lumped parameter formulation instead of a finite-element approach reduces the complexity of the system and time required for mathematical convergence. To improve on the robustness and fidelity of the model and to allow the model to operate under a wide range of parameters, much attention is to be given towards maintaining all the calculations dynamic and time-variant, that is, hard-coded thermodynamic, heat, and fluid flow properties are limited in use and rather calculated on the go based on the system thermodynamic properties such as pressure and temperature. In addition, the two-phase flow nature of saturated steam requires the implementation of a switching mechanism between the desuperheating stage and the condensation stage, as both stages occur hand-in-hand in natural physical phenomena.

For validation, the model will run using input parameters provided by Siemens Energy Inc. and the results of the simulation will be compared to data collected from a reference condenser that is in use at one of Siemens' power plants. However, it must be noted that Siemens does not collect data regarding the transient operation of their condensers. To that end, the condenser's model ability to run dynamically is to be demonstrated by introducing perturbations as step inputs and observing the model's ability to adapt and re-stabilize at a new thermodynamically valid equilibrium position.

1.4 Method

The condenser will be modeled using Siemens Power Plant Automation T3000 (SPPA-T3000) software. The condenser will be modeled using a lumped formulation consisting of three $C\forbar{V}$'s constituting the coolant carrying pipes ($C\forbar{V}_{met}$), the vapor space ($C\forbar{V}_{vap}$), and the condensate liquid ($C\forbar{V}_{liq}$). All three $C\forbar{V}$'s dynamics will be interconnected through heat and mass transfer using appropriate thermodynamic formulation.

In addition, to maintain the system in a dynamic state and ensure compatibility with multiple operating conditions, mathematically and empirically derived equations are used to obtain values for the thermodynamic, heat, and fluid flow properties that are associated with the process of water vapor condensation. Recalling the need for the model to operate in real-time, consideration is given to the setup of the mathematical algorithms used in the computation of said values; for instance, the use of floating point numbers is avoided as much as possible and computed values are re-used whenever appropriate.

CHAPTER 2: BACKGROUND

2.1 Rankine Cycle

A CCPP operates under the principles developed by the Scottish engineer William J.M. Rankine back in 1859 [16]. In an ideal Rankine cycle, water in the liquid phase is passed through a feed pump where its pressure is raised isentropically, that is with no entropy generation. The high pressure water is then fed into the boiler where heat is added isobarically – at a constant pressure – causing the water to vaporize. The water vapor is then superheated by further addition of heat, this ensures that no water droplets form on the steam turbine blades, causing erosion and reducing efficiency. The superheated steam is then expanded isentropically through a steam turbine, inducing shaft rotation and generating energy as it loses pressure and temperature. At the turbine exit, the water vapor is now in the two-phase region with a steam quality greater than 90%. The saturated steam then enters a surface condenser utilizing cooling water, where heat is rejected isobarically at a very low pressure. In a well designed condenser model, the pressure is maintained by at least an order of magnitude below atmospheric conditions, allowing the saturated vapor to condense at the cooling water temperature.

The choice of water as the working fluid in the Rankine cycle is due to its favorable properties such as its non-toxic and nonreactive chemistry, abundance, low cost, and its thermodynamic properties. For instance, water has the highest specific heat of any common substance at $c = 4.19kJ\ kg^{-1}\ k^{-1}$, in addition to its very high heat of vaporization, making it very effective as a cooling medium [17]. Furthermore, the use of water as the working fluid is very advantageous in the Rankine cycle; by condensing the steam from the turbine outlet into liquid inside the condenser, the pressure at the turbine outlet is lowered due to the phase change and the sharp drop in specific volume – $\text{⏑}_f = 1.010 \times 10^{-3}\ m^3\ kg^{-1}$ compared to $\text{⏑}_g = 14.534\ m^3\ kg^{-1}$ at the typical operational values

of $0.1\ bar$ and $319\ K$. This drop in specific volume allows a vacuum to be maintained inside the condenser in addition to increasing the efficiency of the steam turbine.

A generic T-s diagram commonly used in Rankine Cycle calculations is shown in fig. 2.1,

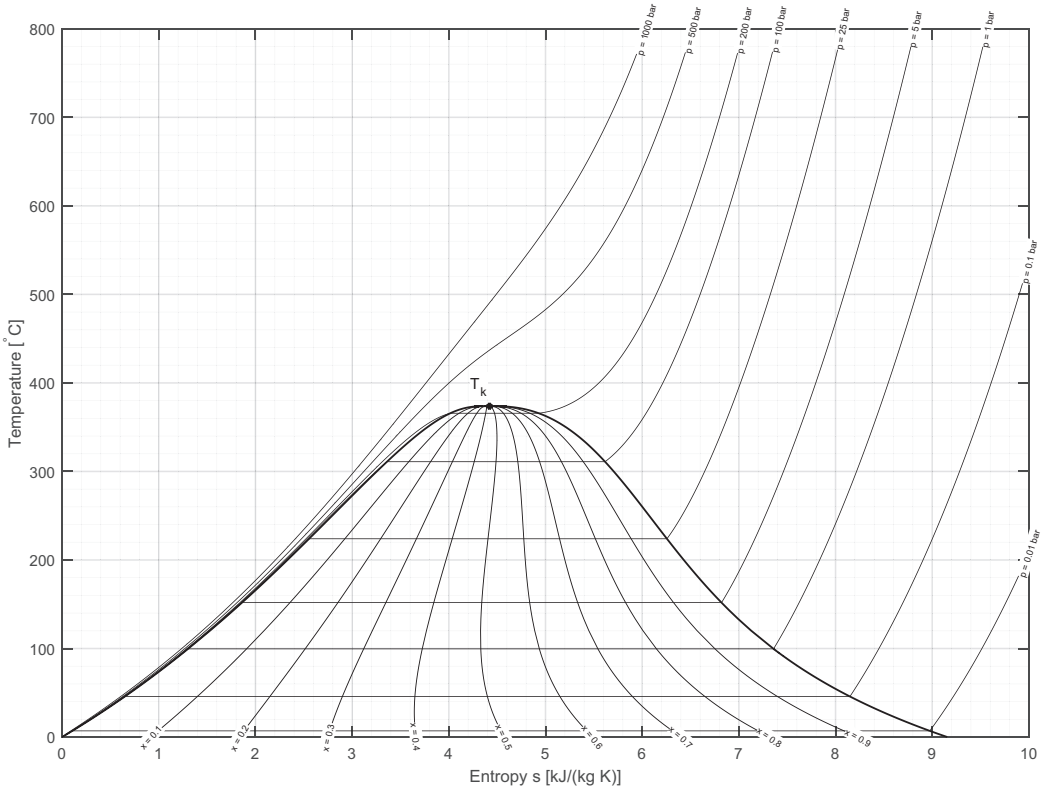

Figure 2.1: T-s diagram

2.2 Steam Condenser

This study is mainly focused on the heat rejection process of the Rankine cycle, more specifically, the steam condenser. Steam condensers are a type of a shell-and-tube heat exchanger that are used in various applications and industries such, but not limited to, HVAC industry, automobile industry,

and refineries. However thermal and nuclear power plants deploy a specific type of heat exchangers known as surface steam condensers. They are named so due to the process at which condensate is formed; cooling water is passed through tube bundles that are placed within the vapor space inside the condenser's shell and as the saturated vapor makes contact with the surface of the tube bundles it gives away the latent heat of vaporization to the coolant switching to a one-phase state consisting of pure liquid water condensate. The condensate then falls off the tube bundles and onto the hotwell due to gravity, where it is then passed to the feed pump to restart the cycle. A generic schematic diagram of a shell-and-tube steam condenser is shown below in fig. 2.2.

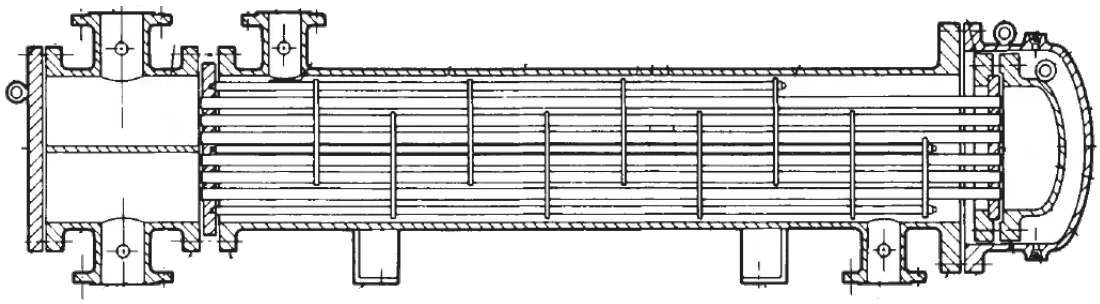

Figure 2.2: Shell-and-Tube Heat Exchanger

2.3 SPPA-T3000

Siemens Power Plant Automation T3000 (SPPA-T3000) is a software developed by Siemens Energy Inc. that is designed for power plant automation, control, reliable operation, and improved performance by giving the right cues to the operation while providing smooth workflows and data display in real-time [18]. The software was not developed with modeling and simulation in mind, however, a previous research done by Caesar [19] proved SPPA-T3000's ability to perform nu-

merical calculations while simulating a transient model of a low-pressure heat recovery steam generator.

The choice of SPPA-T3000 as the modeling and simulation platform is due to the inherent edge that it maintains over many other platforms; it is a visual programming language (VPL) that was designed as a distributed control system (DCS) to be deployed for power plant automation. It contains built-in functions that facilitate the computation of a plethora of thermodynamic properties such as, but not limited to, saturation pressure and temperature, specific enthalpy, specific volume, and specific entropy. It also contains control functions such as, but not limited to, binary/analog logical conjunctions/disjunctions and gate switches, PID control, and delays. As with any other VPL, it also contains mathematical function blocks such as, but not limited to, add, multiply, integrate, differentiate, and so on.

Workflow and implementation of functions in SPPA-T3000 is facilitated with use of block diagrams. A model is generated by interconnecting multiple fundamental function blocks using signal lines in such a manner that a desired operation is performed. An example of a sample calculation is shown in fig. 2.3.

The collection of the function blocks can then be integrated into an embedded diagram where the desired operation is defined as its own function that can be repeatedly used in multiple parts of the model. Embedded diagrams can also be used to organize the model into a hierarchy that consists of, for example, a $C\forall$ at the top level and all of the associated properties and calculations embedded within. An example of an embedded diagram is shown in fig. 2.4.

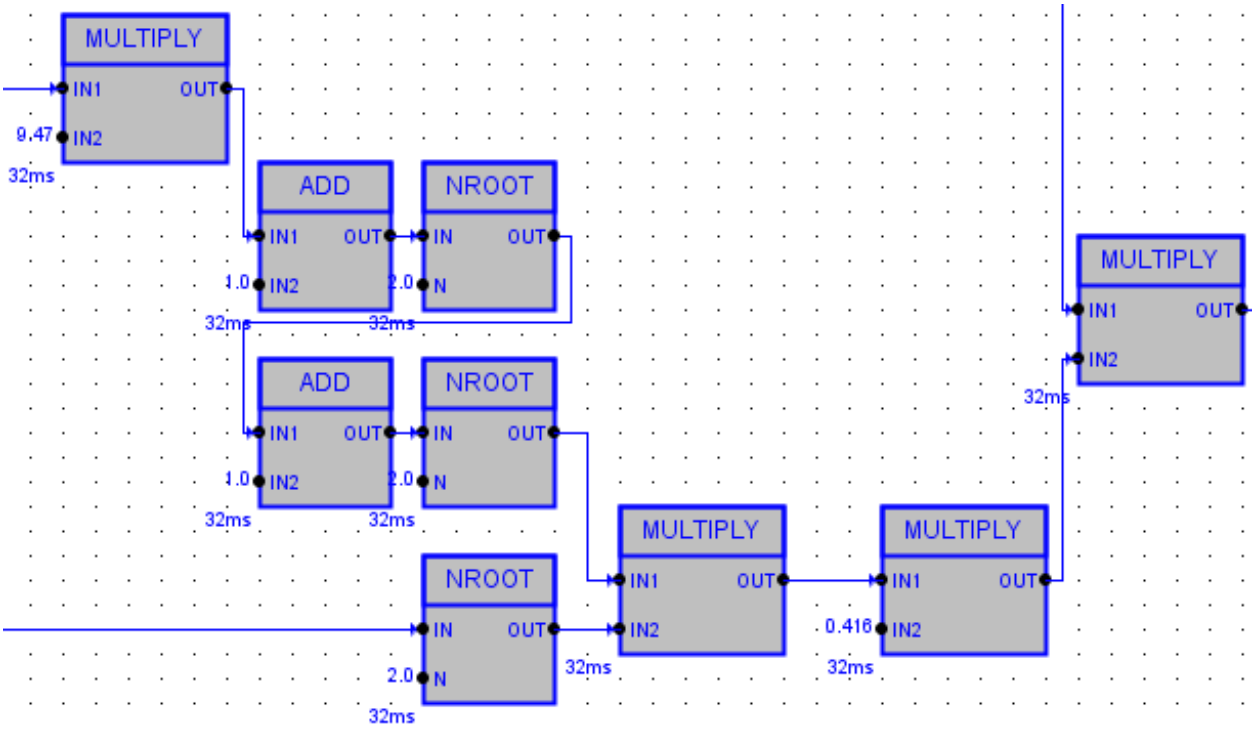

Figure 2.3: Sample collection of function blocks

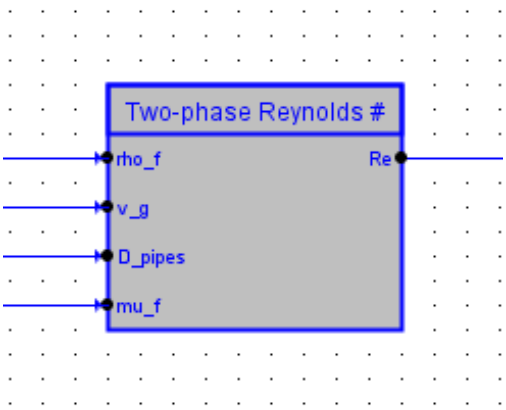

Figure 2.4: Embedded diagram

Another advantage SPPA-T3000 has over other modeling and simulation platforms is the real-time,

continuous operation and analysis of signal inputs and outputs as can be observed in fig. 2.5, in addition to modifying the model during run time without the need for deactivating the simulation. The ease of signal monitoring in real-time facilitates the debugging of the model as signals can be observed and compared to an expected value.

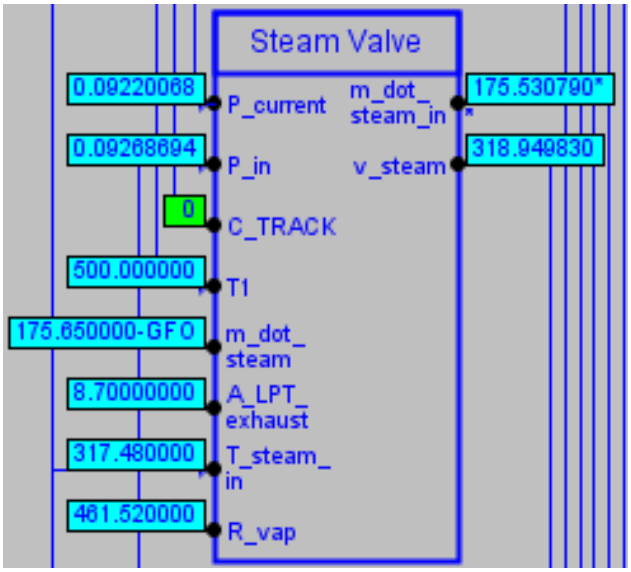

Figure 2.5: Real-time signal input/output display

Lastly, a huge advantage SPPA-T3000 has is its ability to continue operation even when a subsystem fails to operate, for instance when a value is divided by zero, meanwhile generating a visual alarm in place of the faulty signal for ease of pinpointing and debugging the issue.

CHAPTER 3: CONDENSER THERMODYNAMICS AND MODELING

As briefly mentioned in section 1.4, the overall structure of the condenser model consists of three control volumes: (1) $C\not{V}_{met}$, (2) $C\not{V}_{vap}$, and (3) $C\not{V}_{liq}$. In this chapter, the thermodynamic formulation and makeup of each $C\not{V}$ is discussed along with their coupling mechanisms.

3.1 Metal Control Volume ($C\not{V}_{met}$)

In this model, $C\not{V}_{met}$ consists of the coolant carrying pipes as depicted in fig. 3.1. It does not include the condenser body and assumes the interior to be insulated with very low surface emissivity, hence, the condenser body does not exchange energy through any mode. The exterior of condenser is also considered to be insulated and with very low surface emissivity. As such, heat gain from, and loss to, the ambient is neglected. Provided specification of $C\not{V}_{met}$ can be found in table 3.1. Certain geometric parameters that were not provided by Siemens such as the number of pipes (N_{pipe}) were extracted from literature [20].

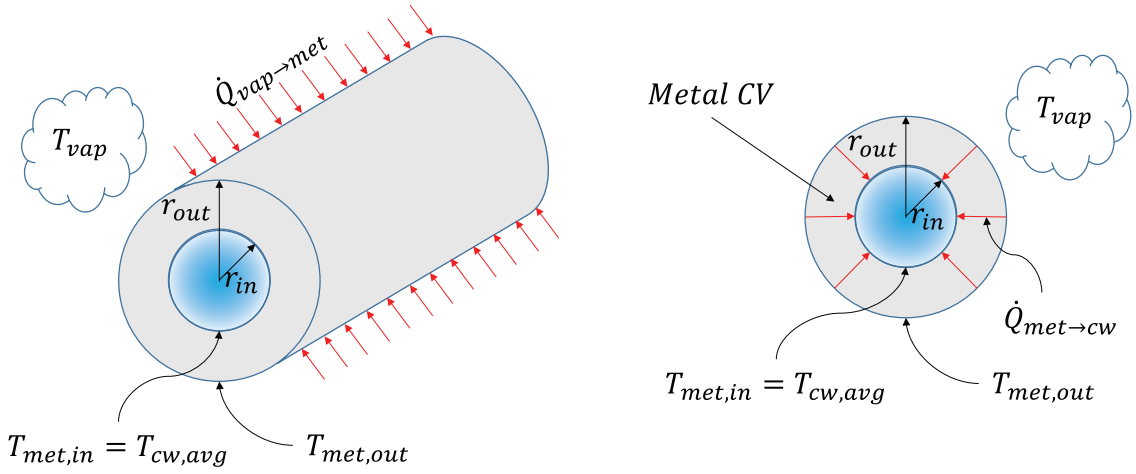

Figure 3.1: Metal Control Volume ($C\not{V}_{met}$)

Table 3.1: Coolant carrying pipes ($C\not{V}_{met}$) specifications

	Parameter	Value	Units
Geometric	N_{pipe}	1500	$-$
	L_{pipe}	20.0	m
	D_{in}	23.0×10^{-3}	m
	D_{out}	25.0×10^{-3}	m
Physical	k_{met}	45.0	$W\ m^{-1}\ K^{-1}$
	ρ_{met}	8000	$kg\ m^{-3}$
	$c_{p,met}$	500	$J\ kg^{-1}\ K^{-1}$
	$c_{p,cw}$	4178	$J\ kg^{-1}\ K^{-1}$
Input	$T_{cw,in}$	*Case dependent*	K
	$\dot{m}_{cw}$	8426.16	$kg\ s^{-1}$

3.1.1 Mathematical Formulation

The governing equation eq. (3.1) for $C\not{V}_{met}$ is derived from first principle as follows,

$$mc_p\dot{T}\Big|_{met} = \dot{Q}_{vap\to met} - \dot{Q}_{met\to cw} \tag{3.1}$$

where m is the mass of the metal making up the pipes, c_v is the specific heat at constant volume, $\dot{T}$ is the change in the temperature of the metal with respect to time, $\dot{Q}_{vap\to met}$ is the convective heat transfer from $C\not{V}_{vap}$ into $C\not{V}_{met}$, and $\dot{Q}_{met\to cw}$ is the convective heat transfer from the inner radius of $C\not{V}_{met}$ and into the circulating cooling water.

To obtain an expression for the dynamic temperature evolution of $C\not{V}_{met}$, we isolate T_{met} by

rearranging eq. (3.1)

$$\dot{T}_{met} = \frac{dT_{met}}{dt} = \frac{\dot{Q}_{vap \to met} - \dot{Q}_{met \to cw}}{m_{met} c_{p,met}} \tag{3.2}$$

To evaluate the expression derived in eq. (3.2), start by expressing a mathematical formulation for $\dot{Q}_{vap \to met}$. By recognizing that heat transfer at the outer boundary is between a solid and a fluid, we apply a boundary condition of the third type at the outer edge of $C\forbar{V}_{met}$

$$-k \left(\frac{\partial T}{\partial \hat{n}} \right)_{r=R_{out}} = H(T_{met,out} - T_{vap}) \tag{3.3}$$

where k is the conductive heat transfer coefficient, H is the convective heat transfer coefficient, $\hat{n}$ is an outward facing unit vector that is normal to the boundary at all points, T_{vap} is the bulk temperature of $C\forbar{V}_{vap}$, and $T_{met,out}$ is the temperature at the outer boundary of $C\forbar{V}_{met}$. Noting that the radial vector and the normal vector both point in the same direction, eq. (3.3) can be rewritten as

$$\dot{Q}_{vap \to met} = H A_{surf,met}(T_{vap} - T_{met,out}) \tag{3.4}$$

The dynamic computation of H and T_{vap} will be discussed in further detail in section section 3.2. As for now, the discussion will only focus on setting up eq. (3.2) and the associated variables. Going back to eq. (3.4), the surface area, $A_{surf,met}$, is directly computed by eq. (3.5)

$$A_{surf,met} = \pi D_{out} L_{pipe} \cdot N_{pipe} \tag{3.5}$$

where π is the physical constant that relates the circle's circumference to its diameter, D_{out} is the outer diameter of the coolant carrying pipes, L_{pipe} is the length of the pipes, and N_{pipe} is the total number of pipes within the condenser. With a mathematical expression for $\dot{Q}_{vap \to met}$ derived, we

turn our attention to $\dot{Q}_{met \to cw}$. Noting that the heat extracted by the coolant is equal to that of the heat conducted through the body of the cooling carrying pipes, we can state the following

$$\dot{Q}_{met,out \to met,in} = \dot{Q}_{met,in \to cw} \tag{3.6}$$

Due to the lumped $C\forall$ formulation, we take the bulk temperature of the cooling water and neglect any local variations of the cooling water temperature along the length of the pipe. Applying a boundary condition of the second type on the inner walls of the coolant carrying pipes, $q''(r = R_{in}, t)$, eq. (3.6) can be expressed as

$$-k \left(\frac{\partial T}{\partial \hat{n}} \right)_{r=R_{in}} = q''(r = R_{in}, t) \tag{3.7}$$

Noting that $\hat{n}$ and the radial vector point in the opposite directions in this case, multiplying both sides by the cross-sectional area, and using the statement used to formulate eq. (3.6), we can express eq. (3.7) as

$$\dot{Q}_{met,out \to met,in} = \dot{Q}_{met,in \to cw} = \frac{2\pi k_{met} L_{pipe} (T_{met} - T_{cw,avg})}{\ln \left({}^{R_{out}}/_{R_{in}} \right)} \cdot N_{pipe} \tag{3.8}$$

where $T_{cw,avg}$ is the average bulk temperature of the cooling water which is obtained from

$$\dot{Q}_{met,in \to cw} = \dot{m}_{cw} dh \tag{3.9}$$

where h is the specific enthalpy. However, recall that dh could be expressed in terms of temperature and specific heat capacity using thermodynamic derivatives as follows

$$c_p \equiv T \left(\frac{\partial s}{\partial T} \right)_{P=cte} = \left(\frac{đq}{dT} \right)_{P=cte} \tag{3.10}$$

where s is the specific entropy, q is the heat transfer into/out of the system, and P is the pressure. However, $đq$ is expressed as

$$đq = du + đw = du + (Pdv) \tag{3.11}$$

where $đw$ is the boundary work, u is the specific internal energy, and du is the differential change in specific internal energy, both of which can be defined as

$$u = h - Pv \longrightarrow du = dh - Pdv - vdP \tag{3.12}$$

plugging eq. (3.12) into eq. (3.11), simplifying, and plugging the result back into eq. (3.10) we get

$$c_p = \left(\frac{dh - \cancel{vdP}^{0;P=cte}}{dT} \right)_{P=cte} = \left(\frac{dh}{dT} \right)_{P=cte} \tag{3.13}$$

rearranging for dh in eq. (3.13) yields

$$dh = c_p dT \tag{3.14}$$

plugging eq. (3.14) into eq. (3.9) yields

$$\dot{Q}_{met,in \to cw} = \dot{m}_{cw} c_p (T_{cw,out} - T_{cw,in}) \tag{3.15}$$

where $\dot{m}_{cw}$ is the cooling water mass flow rate, c_p is water's specific heat at constant pressure, $T_{cw,out}$ is the cooling water temperature leaving the condenser, and $T_{cw,in}$ is cooling water temperature entering the condenser from the cooling towers. However, $T_{cw,in}$ and $\dot{m}_{cw}$ are both constant, thus, eq. (3.15) can be rewritten in terms of $T_{cw,out}$ as in eq. (3.16) which allows the computation of the average cooling water, $T_{cw,avg}$, bulk temperature by taking the arithmetic average of $T_{cw,in}$

and $T_{cw,out}$ as in eq. (3.17)

$$T_{cw,out} = \frac{\dot{Q}_{met,in \to cw}}{\dot{m}_{cw} c_p} + T_{cw,in} \tag{3.16}$$

$$T_{cw,avg} = \frac{T_{cw,in} + T_{cw,out}}{2} \tag{3.17}$$

Lastly, with the lack of information regarding the metal alloy used in the construction of the coolant carrying pipes, it was assumed that the metal is 316 stainless-steel based on Buecker [21], as it is very durable, resists corrosion, and does not deposit contaminants into the fluid stream. The metal mass, m_{met}, is calculated using eq. (3.18)

$$m_{met} = \rho_{met} V_{met} = \pi \rho_{met} L_{pipe} \left(R_{out}^2 - R_{in}^2 \right) \cdot N_{pipe} \tag{3.18}$$

With all the variables defined, the integration of eq. (3.2) with respect to time gives the temperature evolution of $C\cancel{V}_{met}$ as time progresses

$$T_{met}(t) = \int_{t_0}^{t} \frac{\dot{Q}_{vap \to met} - \dot{Q}_{met \to cw}}{m_{met} c_{p,met}} dt + T_{met}(t = t_0) \tag{3.19}$$

A snapshot of $C\cancel{V}_{met}$ modeled in SPPA-T3000 is shown in fig. 3.2.

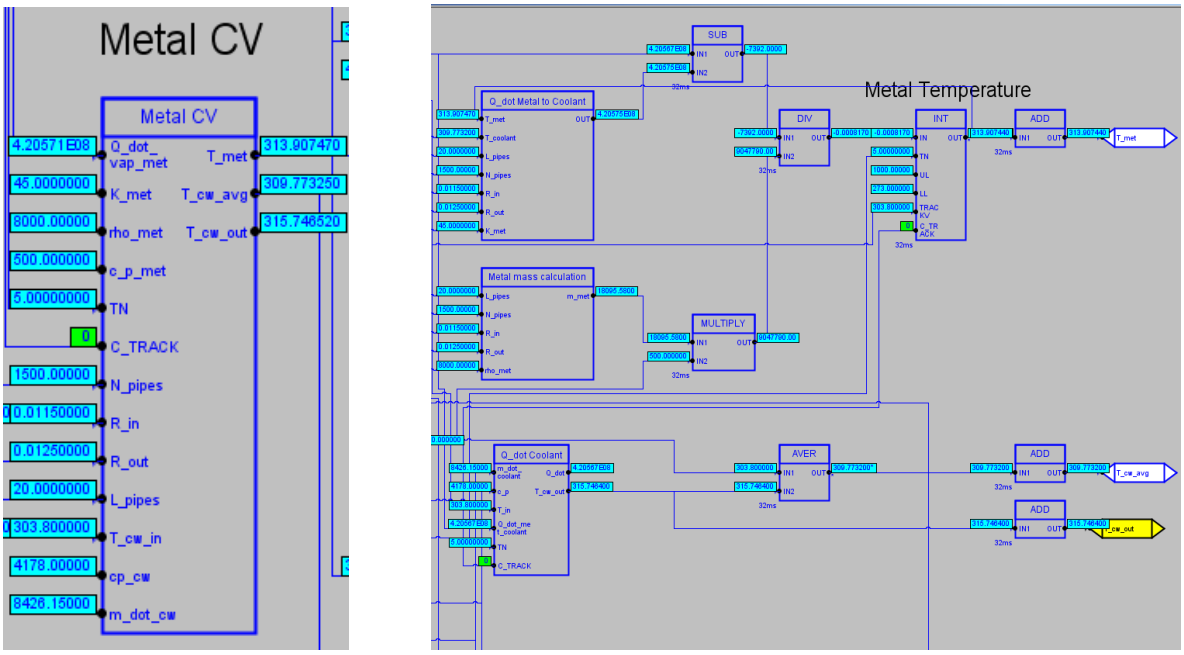

Figure 3.2: Metal Control Volume ($C\not{V}_{met}$) in SPPA-T3000. Top view (left) and 1st level embedded diagram (right)

3.2 Vapor Control Volume ($C\not{V}_{vap}$)

In this model, $C\not{V}_{vap}$ consists of the exhausted steam from the steam turbine. During regular operation, the steam enters the condenser at a saturation quality, χ, that is above 90%. The process of condensation is initiated when the hot vapor comes into contact with the colder surface of $C\not{V}_{met}$, this temperature gradient promotes a directional heat flow from $C\not{V}_{vap}$ into $C\not{V}_{met}$. If enough heat was removed from $C\not{V}_{vap}$, the vapor in contact with $C\not{V}_{met}$ may cool down to below its equilibrium saturation temperature for a given pressure. This now established temperature field — with the minimum temperature being that of $C\not{V}_{met}$ — will promote the formation of condensate [22].

In this analysis, we adopt a film condensation model over an axisymmetric body as opposed to

dropwise condensation model fig. 3.3. The reasons for such choice are twofold, (1) the mechanisms of dropwise condensation remain the subject of debate despite the numerous studies conducted over the years [22], (2) film condensation is naturally more sustainable than dropwise condensation, and thus, the great majority of heat exchangers are designed to operate in that mode [20]. A table indicating all the provided values for $C\not{V}_{vap}$ can be found in table 3.2.

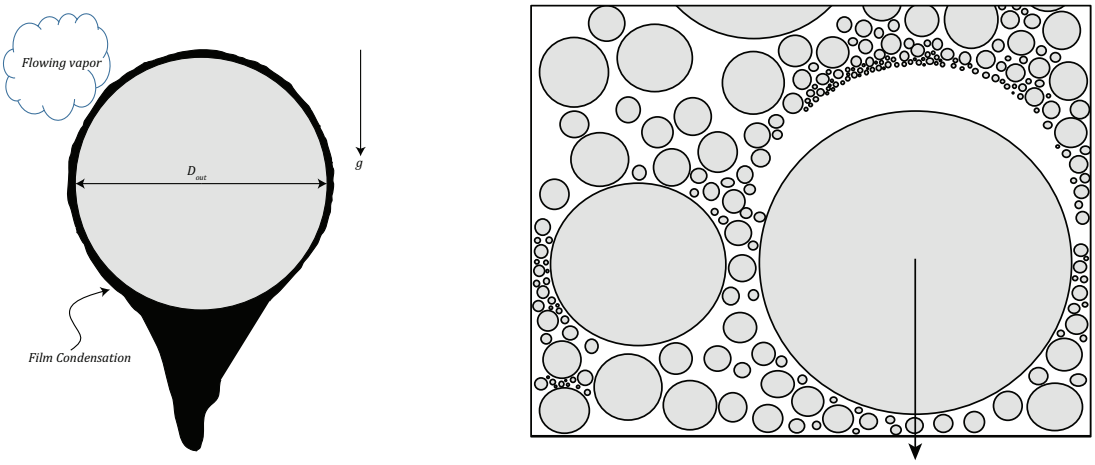

Figure 3.3: Modes of condensation. Film condensation (left) and dropwise condensation (right)

Table 3.2: Vapor space ($C\not{V}_{vap}$) specifications

	Parameter	**Value**	**Units**
Geometric	$\not{V}_{vap}$	$\not{V}_{condenser} - \not{V}_{liq} - \not{V}_{met}$	m^{-3}
Physical	R_{vap}	461.52	$J\ kg^{-1}\ K^{-1}$
Input	T_{vap}	*Case dependent*	K
	P_{vap}	*Case dependent*	bar
	m_{in}	*Case dependent*	$kg\ s{-}1$

3.2.1 Mathematical Formulation

The governing equation for $C\not{V}_{vap}$ is derived from first principle

$$\frac{d}{dt}\left[mu\right]\Big|_{vap} = \Big(\sum_{in}\dot{m}h - \sum_{out}\dot{m}h\Big) + \Big(\sum_{in}\dot{Q} - \sum_{out}\dot{Q}\Big) \tag{3.20}$$

where $\frac{d}{dt}\left[mu\right]\Big|_{vap}$ takes into consideration $C\not{V}_{vap}$'s evolution in terms of mass and energy, $\sum_{in}\dot{m}h$ accounts for the energy mass transfer into $C\not{V}_{vap}$, $\sum_{out}\dot{m}h$ accounts for the energy mass transfer out of $C\not{V}_{vap}$, $\sum_{in}\dot{Q}$ accounts for the heat transfer into $C\not{V}_{vap}$, and lastly $\sum_{out}\dot{Q}$ accounts for the heat transfer out of $C\not{V}_{vap}$.

The left hand side (LHS) of eq. (3.20) can be expanded as

$$\frac{d}{dt}\left[mu\right]\Big|_{vap} = \dot{m}u\Big|_{vap} + m\dot{u}\Big|_{vap} \tag{3.21}$$

where $\dot{m}_{vap}$ is the change in the mass of the vapor space and $\dot{u}_{vap}$ is the change of $C\not{V}_{vap}$'s internal energy. Based on the principle of mass balance, $\dot{m}_{vap}$ can be defined as

$$\dot{m}_{vap} = \dot{m}_{in} - \dot{m}_{V2L} + \dot{m}_{L2V} - \dot{m}_{vp} + \dot{m}_{other} \tag{3.22}$$

where $\dot{m}_{in}$ is the mass flow rate of steam from the turbine's exhaust into the condenser, $\dot{m}_{V2L}$ is the mass flow rate of steam from the vapor phase ($C\not{V}_{vap}$) into the liquid phase ($C\not{V}_{liq}$), $\dot{m}_{L2V}$ is the mass flow rate of flash steam from the liquid phase ($C\not{V}_{liq}$) into the vapor phase ($C\not{V}_{vap}$), $\dot{m}_{vp}$ is the mass flow rate of steam out the vapor space by virtue of the vacuum pump, and $\dot{m}_{other}$ is the mass flow rate of steam into the system by virtue of a miscellaneous process and is only presented for the purposes of generalizing the formulation.

Furthermore, $\dot{u}_{vap}$ can be rewritten in terms of temperature and specific heat capacity using a similar procedure to that used in deriving and expression for dh in eq. (3.14) from section 3.1. Recall that

$$c_{\cancel{v}} = \left(\frac{đq}{dT}\right)_{\cancel{v}=cte} \tag{3.23}$$

from eq. (3.11)

$$đq = du + \cancel{P d\cancel{v}}^{0;\cancel{v}=cte} \tag{3.24}$$

plugging eq. (3.24) into eq. (3.23), rearranging for du, and taking a time derivative on both sides we obtain

$$\dot{u} = c_{\cancel{v}}\dot{T} \tag{3.25}$$

This derived expression, when plugged back into eq. (3.21), allows us to evaluate the temperature evolution of $C\cancel{V}_{vap}$ as a function of time.

Moving on to the right hand side (RHS) of eq. (3.20), we can rewrite the net energy mass transfer, $\left(\sum_{in}\dot{m}h - \sum_{out}\dot{m}h\right)$, as

$$\begin{aligned}\sum_{in}\dot{m}h - \sum_{out}\dot{m}h = \dot{m}h\Big|_{in} + \dot{m}h\Big|_{L2V} + \dot{m}h\Big|_{other} \\ - \dot{m}h\Big|_{V2L} - \dot{m}h\Big|_{vp}\end{aligned} \tag{3.26}$$

The net heat transfer, $\left(\sum_{in}\dot{Q} - \sum_{out}\dot{Q}\right)$, can be generalized using the same procedure used in

eq. (3.26) as

$$\begin{aligned}\sum_{in}\dot{Q}-\sum_{out}\dot{Q} &= -\Big[\ \dot{Q}_{vap\rightarrow met}+\dot{Q}_{vap\rightarrow liq}\Big] \\ &= -\Big[\ HA_{surf}\Big|_{vap\rightarrow met}(T_{vap}-T_{met})+ \\ &\qquad HA_{surf}\Big|_{vap\rightarrow liq}(T_{vap}-T_{liq}\ \ )\Big]\end{aligned} \tag{3.27}$$

where $H_{vap\rightarrow met}$ and $H_{vap\rightarrow liq}$ are the convective heat transfer coefficients between the vapor-metal interface and vapor-liquid interface, respectively.

3.2.2 Convective Heat Transfer Coefficient Estimation

The vapor-metal interface convective heat transfer coefficient is computed using an interpolation formula proposed by Butterworth [23] based on a conservative approach that was introduced by Shekriladze and Gomelauri [24]. In their work, Shekriladze and Gomelauri realized the importance of the mass flow across a condensing surface, they therefore extended on Nusselt's original analysis [25], where Nusselt takes into consideration the effects of interfacial shear boundary condition at the edge of the condensate film, by including the effects of gravity and the approach velocity of the steam.

Based on all previous work discussed, Butterworth suggested the following equation

$$\frac{Nu}{\widetilde{Re}^{1/2}}=0.416\left\{1+(1+9.47F)^{1/2}\right\}^{1/2} \tag{3.28}$$

where Nu is Nusselt's number which is a dimensionless value that describes the ratio of convective heat transfer to conductive heat transfer across a boundary, $\widetilde{Re}$ is the two-phase flow Reynold's

number which is a dimensionless value that describes the ratio of inertial forces to viscous forces that involves the vapor velocity and the condensate properties, and lastly F is a dimensionless quantity that is a measure of the relative effects of the gravitational and velocity fields on the process. All three equations are expressed mathematically in eq. (3.29), eq. (3.30), and eq. (3.31), respectively.

$$Nu = \frac{H}{k_f/L_c} = \frac{HL_c}{k_f} \tag{3.29}$$

$$\widetilde{Re} = \frac{\rho_f v_g L_c}{\mu_f} \tag{3.30}$$

$$F = \frac{gD\mu_f h_{fg}}{{v_g}^2 k_f \Delta T} \tag{3.31}$$

where H is the convective heat transfer coefficient, k_f is the conductive heat transfer coefficient of the condensate film, L_c is the characteristic length (which is the diameter, D_{out}, in case of an external flow over a cylinder), ρ_f is the density of the condensate film, v_g is the approach velocity of the steam, μ_f is the dynamic viscosity of the condensate film, g is the physical constant that quantifies gravitational acceleration, h_{fg} is the latent heat of vaporization, and $\Delta T = T_{sat} - T_{met}$ is the difference between the saturation temperature of the incoming steam and the cooling surface temperature.

Isolating the convective heat transfer coefficient from eq. (3.28) yields

$$H_{vap \to met} = \frac{0.416 k_f}{D_{out}} \left\{1 + (1 + 9.47F)^{1/2}\right\}^{1/2} \widetilde{Re}^{-1/2} \tag{3.32}$$

In the spirit of maintaining the model as dynamic as possible, data from Dortmund Data Bank (DDB) [26], the world's largest factual data bank for thermophysical properties of pure components

and their mixtures, was used to extrapolate a temperature dependent dynamic viscosity, μ_f, for the condensate film. The fitted equation is in the form of

$$\mu_f = \mu_f\left(T_{avg}\right) = A \cdot 10^{\frac{B}{T_{avg} - C}}, \text{ where } \begin{cases} A = 2.44 \times 10^{-5} Pa \cdot s \\ B = 247.8K \\ C = 140.0K \end{cases} \tag{3.33}$$

In addition to the dynamic viscosity, the thermal conductivity, k_f, of the condensate film was also fitted by Kays [27] and extrapolated as a function of temperature. The fitted equation is in the form of

$$k_f = k_f\left(T_{avg}\right) = A \cdot {T_{avg}}^2 + B \cdot T_{avg} + C, \text{ where } \begin{cases} A = -8.354 \times 10^{-6} \\ B = \quad 6.530 \times 10^{-3} \\ C = -0.598 \end{cases} \tag{3.34}$$

where T_{avg} in eq. (3.33) and eq. (3.34) is the condensate film temperature and is computed to be the arithmetic average of vapor bulk temperature, T_{vap}, and the condensing interface temperature, T_{met}, as is shown in eq. (3.35).

$$T_{avg} = \frac{T_{vap} + T_{met}}{2} \tag{3.35}$$

A multitude of different formulations and models that are higher in complexity than eq. (3.28) do exist in the literature and are discussed in detail by Rose [28]. However, as can be observed in

fig. 3.4, experimental data that was collected by other researchers [29–40] was compiled by Rose [28] and compared against eq. (3.28) predictions and the original work presented by Nusselt [25].

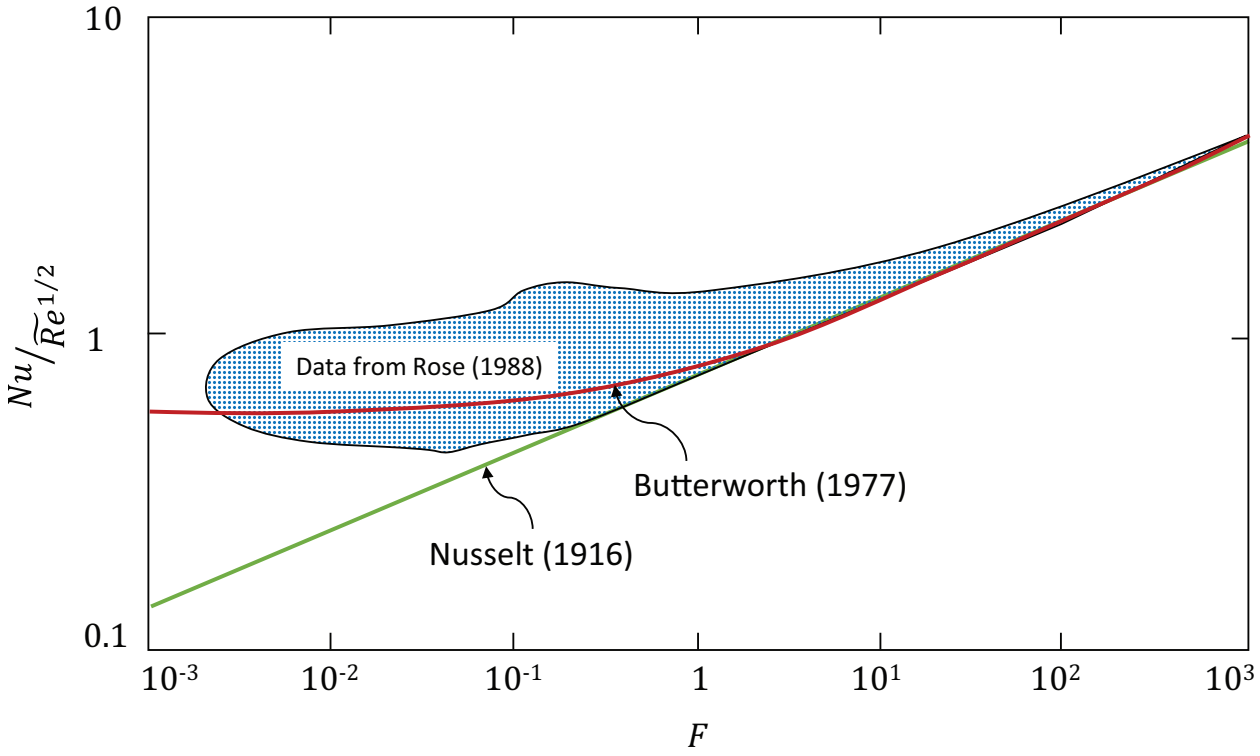

Figure 3.4: Experimental data vs. Butterworth [23] model (adapted from Rose [28])

From fig. 3.4, a huge spread in the data can be noted at high velocities (low F), nonetheless, since the proposed model falls nicely in the band of experimental data, the use of a more complex numerical model to compute the convective heat transfer coefficient, H, is not justified as that would demand more computational power, which in turn translates to more CPU time, deviating the model away from real-time operation. For such reasons, the model proposed by Butterworth [23] in eq. (3.28) was then deemed appropriate for use in the modeling of the condenser in this research.

Although the model presented by Butterworth is conservative in predicting condensation in many situations with reasonable accuracy, Hewitt [41] incorporated a correction factor to the convective

heat transfer coefficient, H, computed using eq. (3.28). This correction factor accounts for the additional effect of vapor superheat.

3.2.3 Superheat Correction Factor

In many practical cases, the condensing vapor is at a quality, χ, of no less than 90%. However, at times, the condensing vapor might enter the condenser at the borderline of being saturated and superheated. The vapor is condensed on the interface of $C\forall_{met}$, yet, the condensing steam needs to reject the slight excess in heat and cool down from the bulk temperature, T_{vap}, to the saturation temperature at the interface, T_{sat}. Given that the steam is at the borderline of saturation and superheat, the effect of superheat is usually small, notwithstanding, it can be corrected for using the expression derived by Hewitt [41] presented in eq. (3.36)

$$H_{corrected} = H\left(1-\zeta\right)^{1/2} \tag{3.36}$$

where ζ is defined in eq. (3.37) as

$$\zeta = \frac{c_{p,g}\left(T_{vap}-T_{sat}\right)}{h_{fg}} \tag{3.37}$$

Once again, to maintain as dynamic as possible, and based on the work done by Vestfálová and Šafaík [42], regression of the International Association for the Properties of Water and Steam - Formulation 1995 (IAPWS-95) data gave rise to an approximate, yet reasonably accurate functional dependence of the isobaric specific heat capacity of water vapor, $c_{p,g}$, on pressure and temperature.

The proposed equation is in the form of

$$c_{p,g} = c_{p,vap}\left(P,T\right) = E\left(T\right) + F\left(T\right)\left(P - P_{tr}\right)$$
$$P_{tr} = 611.657Pa \tag{3.38}$$

where T is the temperature of the vapor in $°C$, P_{tr} is the triple point pressure ($611.657Pa$ for water), which is the lowest pressure at which all three phases of matter co-exist in equilibrium. Furthermore, $E\left(T\right)$ and $F\left(T\right)$ presented in eqs. (3.39) and (3.40) are both temperature dependent parameters that correspond to the isobaric heat capacity at a pressure equal to the triple point pressure and describe the slope of growth of the isobaric heat capacity with an increase in pressure, respectively.

$$E\left(T\right) = A_E + B_E T + C_E T^2 \tag{3.39}$$

$$F\left(T\right) = \frac{1}{A_F + B_F T + C_F T^2} \tag{3.40}$$

The values for the coefficients of the polynomial regression are tabulated for the sake of completeness and are presented in table 3.3.

The regression equation permits the evaluation of the isobaric heat capacity of water vapor in a temperature range of $0°C$ - $200°C$ ($273K$ - $473K$) and a pressure range of $611.657Pa$ - $200KPa$ with a deviation of less than 1.2% from the values computed using the IAPWS-95 formulation as can be observed from Table 3 in [42]. Furthermore, for the typical range of condenser operating pressures ($0.04bar$ - $0.1bar$), the maximum deviation can be observed to be 0.17%, hence, indicating that the values obtained from the regression polynomial are accurate and very reliable for usage in the condenser model.

Table 3.3: Coefficients of regression polynomial for $E\,(T)$ and $F\,(T)$

	$T < 50°C$	$T > 50°C$	$Units$
A_E	1877.2	1856.1	$m^2\ s^{-2}\ K^{-1}$
B_E	-0.49545	0.28056	$m^2\ s^{-2}\ K^{-2}$
C_E	8.1818×10^{-3}	6.9444×10^{-4}	$m^2\ s^{-2}\ K^{-3}$
A_F	22.537	22.537	$kg\ K\ m^{-3}$
B_F	0.49321	0.49321	$kg\ m^{-3}$
C_F	0.048927	0.048927	$kg\ K^{-1}\ m^{-3}$

Note that embedded function diagram designated to compute $c_{p,vap}$ required values to be in $°C$ for the temperature and Pa for the pressure in accordance to the regression polynomial. Moreover, the embedded function diagram used an analog transfer switch (AFXR) to dictate which values of the regression polynomial coefficients are to be used for calculation based on what temperature regime the vapor is currently in ($T < 50°C$ or $T > 50°C$).

Lastly, with $c_{p,vap}$ computed, a value for $c_{\not{v},vap}$ can be obtained for usage in eq. (3.25) and any subsequent equation that utilizes the value by subtracting the vapor gas constant, R_{vap}, from the computed $c_{p,vap}$ value. This approach of computing $c_{\not{v},vap}$ is valid as long as the pressure is around or below $0.1bar$ $(10kPa)$, regardless of the temperature, since approximating water vapor as an ideal gas yields a negligible error of less than 0.1% [43].

A mathematical expression is shown in eq. (3.41)

$$c_{\not{v},vap} = c_{p,vap} - R_{vap} \tag{3.41}$$

A snapshot of the embedded diagram with can be seen in [Fig. 3.5].

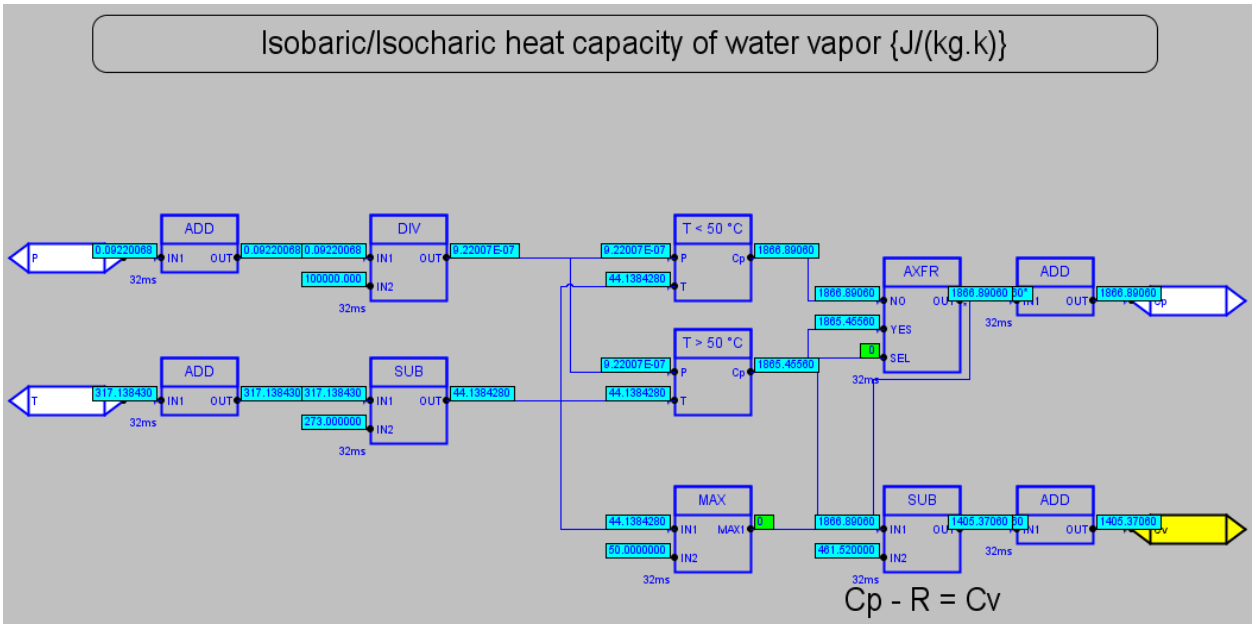

Figure 3.5: $c_{p,vap}$ and $c_{\cancel{v},vap}$ computation logic

3.2.4 Temperature Evolution and Mass Transfer

With everything defined, we go back to the governing eq. (3.20) and redefine it using eqs. (3.21), (3.22) and (3.25) to (3.27) as

$$\begin{aligned} m_{vap}c_{\cancel{v},vap}\dot{T}_{vap} = \dot{m}_{in} \quad (h_{in} \quad - u_{vap}) - \dot{m}_{vp} \quad (h_{vp} \quad - u_{vap}) + \\ \dot{m}_{L2V} \ (h_{L2V} \ - u_{vap}) - \dot{m}_{V2L} \ (h_{V2L} \ - u_{vap}) + \\ \dot{m}_{other} \ (h_{other} - u_{vap}) + \dot{Q}_{Net} \end{aligned} \tag{3.42}$$

Equation (3.42) can now be solved for $\dot{T}_{vap}$ and $\dot{m}_{V2L}$. From the T-s diagram found in fig. 2.1, note that when the vapor is not within the dome but rather to the right of the saturation line, heat rejection will cause the temperature to drop at a constant pressure line but cause no condensation

until the vapor temperature reaches the dew point temperature, which is defined as the saturation temperature for a phase change in the direction of vapor to liquid. At that point, mass transfer occurs and a sharp drop in specific volume due to the phase-change from vapor to liquid causes the pressure to drop. This reduced pressure places the vapor further away from the dew point temperature at that pressure, causing the previously described process to repeat once again. A pictorial representation of the process can be found in fig. 3.6.

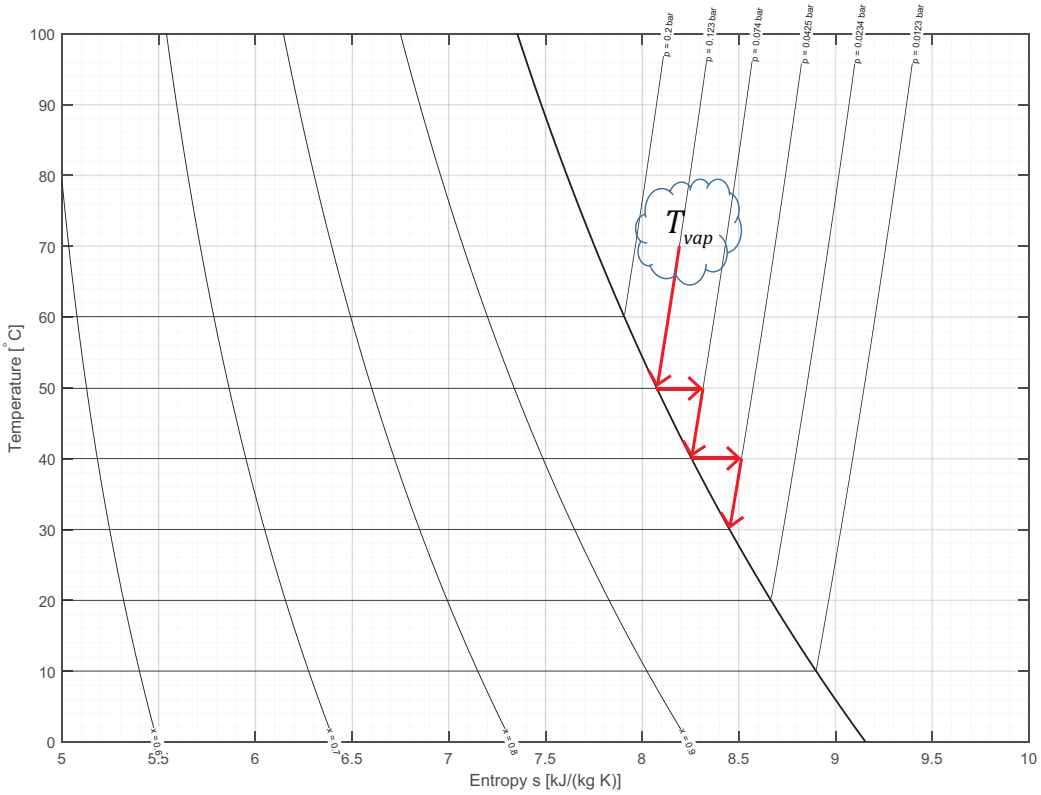

Figure 3.6: Close-up of T-s diagram – cooling mode

This process is expressed mathematically in eq. (3.43)

$$T_{vap} > T_{dp}\left(P_{vap}\right) + \varepsilon \longrightarrow \dot{m}_{V2L} = 0 \; and \; \dot{T}_{vap} < 0 \tag{3.43}$$

where ε is a small deviation in the vicinity of the value in question used for numerical stability. In this model, ε was chosen to be 1% of the dew point temperature, that is $\varepsilon = 0.01 T_{dp}\left(P_{vap}\right)$.

Expanding on the previous case, if the vapor is at the dew point temperature and is within an upper and lower limit (i.e a deadband), the vapor will condense at constant temperature. The change in specific volume from vapor to liquid will push the vapor to a lower pressure, and hence, into a new dew point temperature, triggering the scenario expressed in eq. (3.43). In the limit that the system reaches a steady-state, the model will predominantly operate under condensing mode. This occurs when a phase change pushes the vapor to a lower pressure, but at the same time, incoming steam pressurizes the condenser, pushing the vapor into a higher pressure. Over time, these oscillations around the dew point temperature damp out as the system reaches steady-state. A pictorial representation of the process on the T-s diagram can be found in fig. 3.7.

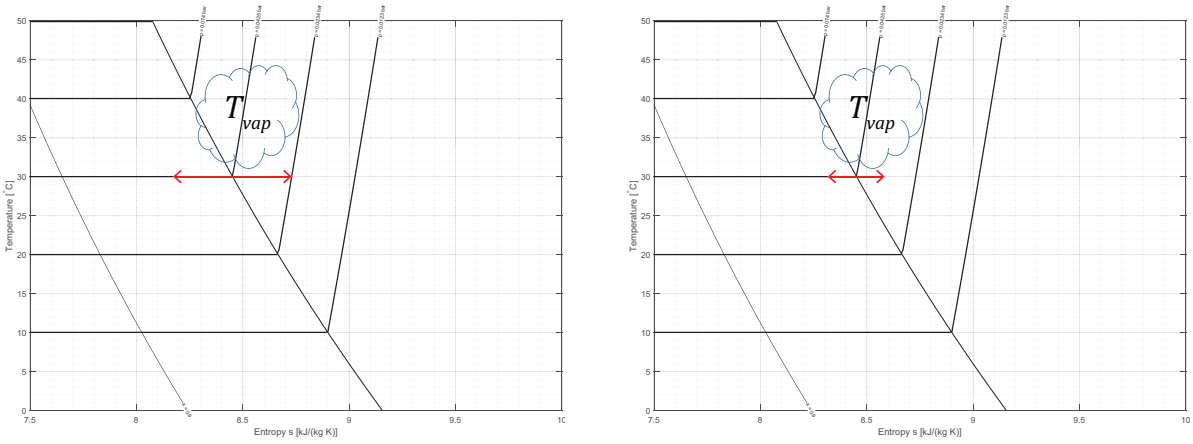

Figure 3.7: Condensing mode. Initial oscillatory behavior (left) and steady-state operation (right)

The process is expressed mathematically in eq. (3.44)

$$T_{vap} \approx T_{dp}\left(P_{vap}\right) \pm \varepsilon \longrightarrow \dot{m}_{V2L} > 0 \; and \; \dot{T}_{vap} = 0 \tag{3.44}$$

Alternatively, during the transient time where the vapor is contained within the dome of the T-s diagram and heat is being rejected, the quality of the steam χ, decreases at a constant temperature while mass transfer from $C\forall_{vap}$ to $C\forall_{liq}$ takes place. As the vapor condenses and mass transfer takes place , a drop in pressure due to a sharp drop in specific volume of the vapor occurs. The incoming steam with a higher energy content serves to heat up the the vapor found within the condenser, increasing the temperature ever so slightly, in addition to pressurizing the system, both of which cause the equilibrium point to shift. This slight increase in temperature and pressure will trigger either one of the previous scenarios described in eqs. (3.43) and (3.44).

The process is expressed mathematically in eq. (3.45)

$$T_{vap} < T_{dp}\left(P_{vap}\right) - \varepsilon \longrightarrow \dot{m}_{V2L} > 0 \; and \; \dot{T}_{vap} > 0 \tag{3.45}$$

A schematic of all the controls logic is found in fig. 3.8.

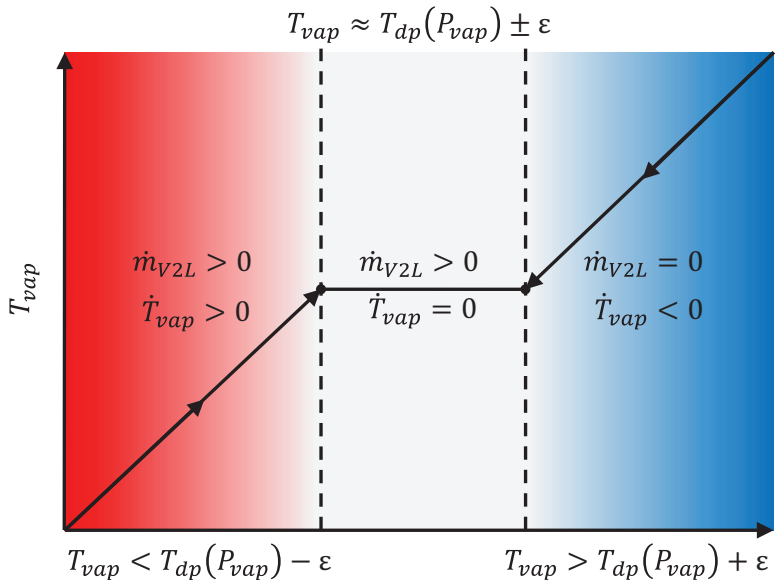

Figure 3.8: Switching logic schematic

With these scenarios defined, eq. (3.42) can be used to solve for either of these cases as follows

- Cooling mode: find the temperature response by setting $\dot{m}_{V2L} = 0$ while allowing $\dot{T}_{vap}$ to vary.
- Condensing mode: find the mass transfer response by setting $\dot{T}_{vap} = 0$ while allowing $\dot{m}_{V2L}$ to vary.
- Combined mode: find both responses by allowing both values, $\dot{m}_{V2L}$ and $\dot{T}_{vap}$, to vary, where $\dot{m}_{V2L}$ is obtained from condensing mode.

Let

$$\begin{aligned} E_{in} &= \dot{m}_{in} (h_{in} - u_{vap}) \\ E_{vp} &= \dot{m}_{vp} (h_{vp} - u_{vap}) \\ E_{L2V} &= \dot{m}_{L2V} (h_{L2V} - u_{vap}) \\ E_{V2L} &= \dot{m}_{V2L} (h_{V2L} - u_{vap}) \\ E_{other} &= \dot{m}_{other} (h_{other} - u_{vap}) \end{aligned}$$

Then, the equation governing the cooling mode described by eq. (3.43) is

$$\dot{T}_{vap} = \frac{E_{in} - E_{vp} + E_{L2V} + E_{other} + \dot{Q}_{Net}}{m_{vap} c_{\cancel{v},vap}} \tag{3.46}$$

integrating eq. (3.46) yields

$$T_{vap}(t) = \int_{t_0}^{t} \frac{E_{in} - E_{vp} + E_{L2V} + E_{other} + \dot{Q}_{Net}}{m_{vap} c_{\cancel{v},vap}} dt + T_{vap}(t = t_0) \tag{3.47}$$

As for the condensing mode described in eq. (3.44), the governing equation is

$$\dot{m}_{V2L} = \frac{E_{in} - E_{vp} + E_{L2V} + E_{other} + \dot{Q}_{Net}}{(h_{vp} - u_{vap})} \tag{3.48}$$

with $\dot{m}_{V2L}$ now known, the integration of eq. (3.22) permits us to compute the amount of vapor within the condenser, yielding

$$m_{vap} = \int_{t_0}^{t} (\dot{m}_{in} - \dot{m}_{V2L} + \dot{m}_{L2V} - \dot{m}_{vp} + \dot{m}_{other})\, dt + m_{vap}(t = 0) \tag{3.49}$$

Lastly, the governing equation describing the scenario depicted by eq. (3.45) is

$$\dot{T}_{vap} = \frac{E_{in} - E_{vp} + E_{L2V} - E_{V2L} + E_{other} + \dot{Q}_{Net}}{m_{vap} c_{\forall, vap}} \tag{3.50}$$

where $\dot{m}_{V2L}$ is obtained from the calculations computed in the condensing mode described in eqs. (3.44) and (3.48). Integrating eq. (3.50) yields

$$T_{vap}(t) = \int_{t_0}^{t} \frac{E_{in} - E_{vp} + E_{L2V} - E_{V2L} + E_{other} + \dot{Q}_{Net}}{m_{vap} c_{\forall, vap}} dt + T_{vap}(t = t_0) \tag{3.51}$$

A schematic of the switching logic from the SPPA-T3000 interface is shown in fig. 3.9.

3.3 Liquid Control Volume ($C\forall_{liq}$)

The last $C\forall$ that is contained within this model is $C\forall_{liq}$. The condensate liquid found at the bottom of the condenser, or the hotwell, comprises the majority of the feedwater that runs through the

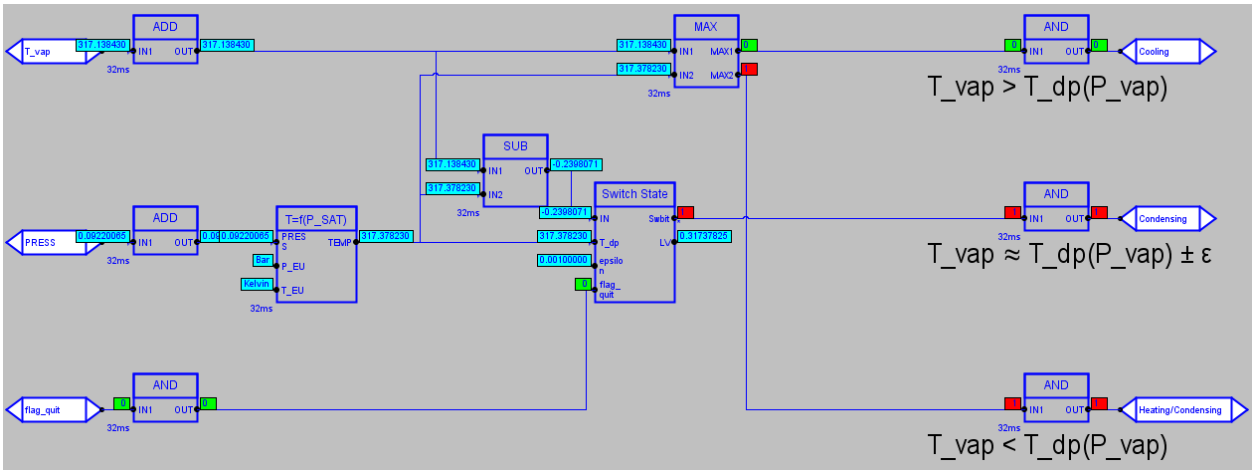

Figure 3.9: Switching logic in SPPA-T3000

heat recovery steam generator (HRSG) during operation and standby (a wet layup) as per the guidelines issued by a number of industry organizations including, but not limited to, ASME, EPRI, and VGB Powertech e.V. [44–46] indicating that all water-touched surfaces remain immersed during the standby period.

Table 3.4: Condensate liquid ($C\forall_{liq}$) specifications

	Parameter	**Value**	**Units**
Geometric	$\forall_{liq,max}$	81.75	m^{-3}
	$\forall_{liq,avg}$	67.55	m^{-3}
	$\forall_{liq,min}$	3.73	m^{-3}
Physical	$c_{p,liq}$	4180.1	$J\ kg^{-1}\ K^{-1}$
Input	$T_{liq,init}$	*Case dependent*	K
	P_{vap}	*Case dependent*	bar

From the data provided by Siemens Energy Inc. it was noted that the system would trip, or halt activity, if the water level reaches the minimum or maximum values tabulated in table 3.4. In

order to prevent condensate accumulation, a simple PI controller was implemented to simulate the pumping of the condensate back into the Rankine cycle for heat addition. However, it must be noted that the controller design is outside of the scope of the research, and as such, its dynamics were ignored.

3.3.1 Mathematical Formulation

The governing equation for $C\forbar{V}_{met}$ is

$$\frac{d}{dt}\left[mu\right]\Big|_{liq} = \Big(\sum_{in}\dot{m}h - \sum_{out}\dot{m}h\Big) + \Big(\sum_{in}\dot{Q} - \sum_{out}\dot{Q}\Big) \tag{3.52}$$

where $\frac{d}{dt}\left[mu\right]\Big|_{liq}$ takes into consideration $C\forbar{V}_{liq}$'s evolution in terms of mass and energy, $\sum_{in}\dot{m}h$ accounts for the energy mass transfer into $C\forbar{V}_{liq}$, $\sum_{out}\dot{m}h$ accounts for the energy mass transfer out of $C\forbar{V}_{liq}$, $\sum_{in}\dot{Q}$ accounts for the heat transfer into $C\forbar{V}_{liq}$, and lastly $\sum_{out}\dot{Q}$ accounts for the heat transfer out of $C\forbar{V}_{liq}$.

The left hand side (LHS) of eq. (3.52) can be expanded as

$$\frac{d}{dt}\left[mu\right]\Big|_{liq} = \dot{m}u\Big|_{liq} + m\dot{u}\Big|_{liq} \tag{3.53}$$

where $\dot{m}_{liq}$ is the change in the mass of the condensate liquid and $\dot{u}_{liq}$ is the change of $C\forbar{V}_{liq}$'s internal energy. Based on the principle of mass balance, $\dot{m}_{liq}$ can be defined as

$$\dot{m}_{liq} = \dot{m}_{V2L} - \dot{m}_{L2V} - \dot{m}_{out} + \dot{m}_{other} \tag{3.54}$$

where $\dot{m}_{V2L}$ is the mass flow rate of steam from the vapor phase ($C\forbar{V}_{vap}$) into the liquid phase ($C\forbar{V}_{liq}$), $\dot{m}_{L2V}$ is the mass flow rate of flash steam from the liquid phase ($C\forbar{V}_{liq}$) into the vapor

phase ($C\cancel{V}_{vap}$), $\dot{m}_{out}$ is the mass flow rate of the hotwell condensate out the condensate liquid $C\cancel{V}$ by virtue of the feedwater pump, and $\dot{m}_{other}$ is the mass flow rate of condensate liquid into the system by virtue of a miscellaneous process.

Furthermore, from eq. (3.25), we can rewrite $\dot{u}_{liq}$ in terms of specific heat and change in temperature, allowing us to evaluate the temperature evolution of $C\cancel{V}_{liq}$. The net energy mass transfer, $\left(\sum_{in}\dot{m}h - \sum_{out}\dot{m}h\right)$, on the RHS of eq. (3.52) can be expanded to

$$\begin{aligned}\sum_{in}\dot{m}h - \sum_{out}\dot{m}h = \quad & \dot{m}h\Big|_{V2L} + \dot{m}h\Big|_{other} \\ & - \dot{m}h\Big|_{L2V} - \dot{m}h\Big|_{out}\end{aligned} \tag{3.55}$$

and the net heat transfer, $\left(\sum_{in}\dot{Q} - \sum_{out}\dot{Q}\right)$, on the RHS of eq. (3.52) can be generalized in the same manner as follows

$$\begin{aligned}\sum_{in}\dot{Q} - \sum_{out}\dot{Q} &= \dot{Q}_{vap\rightarrow liq} \\ &= HA_{surf}\Big|_{vap\rightarrow liq}(T_{vap} - T_{liq})\end{aligned} \tag{3.56}$$

3.3.2 Temperature Evolution and Mass Transfer

With the governing equation fully defined, we use the results from eqs. (3.53) to (3.56) to rewrite eq. (3.52) as follows

$$\begin{aligned}m_{liq}c_{\cancel{v},liq}\dot{T}_{liq} = \dot{m}_{V2L}\ (h_{V2L}\ - u_{liq}) - \dot{m}_{L2V}\ (h_{L2V}\ - u_{liq}) + \\ \dot{m}_{other}\,(h_{other} - u_{liq}) - \dot{m}_{out}\ \ (h_{out}\ \ - u_{liq}) + \dot{Q}_{Net}\end{aligned} \tag{3.57}$$

Equation (3.57) can now be solved for $\dot{T}_{liq}$ and $\dot{m}_{L2V}$, where $\dot{T}_{liq}$ is the temperature evolution of $C\cancel{V}_{liq}$, and $\dot{m}_{L2V}$ is the rate of mass transfer from $C\cancel{V}_{liq}$ to $C\cancel{V}_{vap}$. The thermodynamics and justification behind the implementation of this mode of mass transfer is discussed in further detail in section 3.3.3.

From the T-s diagram found in fig. 2.1, if the condensate liquid is at a lower pressure than the vapor above it, the only mode of mass transfer would be through condensation from $C\cancel{V}_{vap}$ into $C\cancel{V}_{liq}$, which was discussed in detail in section 3.2. However, the temperature of the liquid is not constrained, as it may increase or decrease due to heat addition/extraction and the pumping of the condensate out of the condenser. Therefore

$$P_{liq} = P_{sat}\left(T_{liq}\right) < P_{vap} \longrightarrow \dot{m}_{L2V} = 0 \; and \; \dot{T}_{liq} \neq 0 \tag{3.58}$$

Let

$$\begin{aligned} E_{L2V} &= \dot{m}_{L2V}\ (h_{L2V} - u_{liq}) \\ E_{V2L} &= \dot{m}_{V2L}\ (h_{V2L} - u_{liq}) \\ E_{out} &= \dot{m}_{out}\ (h_{out} - u_{liq}) \\ E_{other} &= \dot{m}_{other}\,(h_{other} - u_{liq}) \end{aligned}$$

where $h_{L2V} = h_g(T_{liq})$, $h_{V2L} = h_f(T_{vap})$, and $h_{out} = h_f(T_{liq})$. Enforcing the condition of $\dot{m}_{L2V} = 0$ and solving for $\dot{T}_{liq}$ in eq. (3.57) yields

$$\dot{T}_{liq} = \frac{E_{V2L} - E_{out} + E_{other} + \dot{Q}_{Net}}{m_{liq} c_{\cancel{v},liq}} \tag{3.59}$$

With E_{V2L} being computed in $C\cancel{V}_{vap}$, E_{out} and E_{other} being known, integrate both sides of

eq. (3.59) to obtain the temperature of $C\forall_{liq}$.

$$T_{liq}(t) = \int_{t_0}^{t} \frac{E_{V2L} - E_{out} + E_{other} + \dot{Q}_{Net}}{m_{liq} c_{\forall,liq}} dt + T_{liq}(t = t_0) \tag{3.60}$$

3.3.3 Flash Steam

Flash steam is a name given to the phenomenon where water in liquid form changes state to gaseous form when pressure is reduced drastically. It is no different than "normal/conventional" steam, it is simply named as such as a convenience to better explain how the steam was formed; normal steam occurs when feedwater passing through the HRSG components gets heated beyond saturation conditions, whereas flash steam occurs when the condensate found in the hotwell of the condenser experiences a drastic pressure drop as the vacuum pump pumps out non-condensables (air) during start-up, for example.

This phenomenon can also be explained from an equilibrium standpoint. From a thermodynamic view, all systems defined at an equilibrium state have the following property: The values assumed by the extensive parameters in the absence of an internal constraint are those that maximize the entropy over the manifold of constrained equilibrium states [47].

To further elaborate, take for instance a closed system consisting of two partitions separated by a movable wall that is impervious to the flow of matter as depicted in fig. 3.10. Let the number of moles be fixed and constant, however, allow for $U^{(1)}$ and $U^{(2)}$ along with $\forall^{(1)}$ and $\forall^{(2)}$ to vary subject to the limits of the closed system

$$U^{(1)} + U^{(2)} = constant \tag{3.61}$$

and

$$\not{V}^{(1)} + \not{V}^{(2)} = constant \tag{3.62}$$

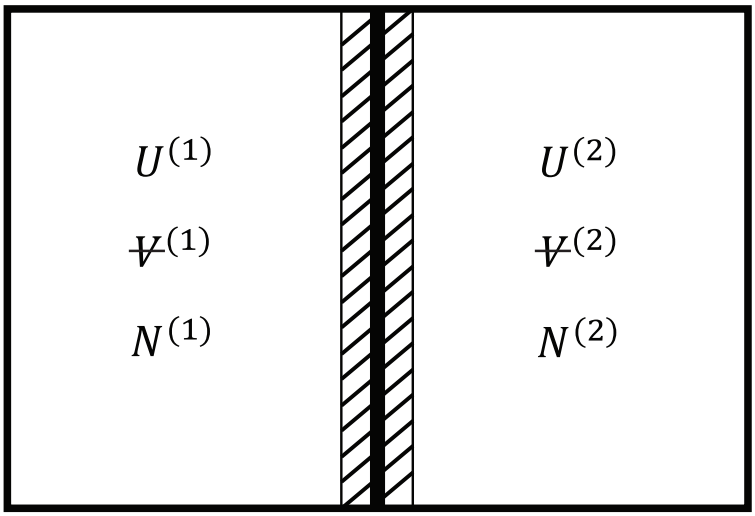

Figure 3.10: Closed 2 partitions system

We now remove the internal constraint (the wall) and allow for the system to evolve. The extremum principle requires that no change in entropy result from infinitesimal processes

$$dS = 0$$

where

$$\begin{aligned} dS = &\left(\frac{\partial S^{(1)}}{\partial U^{(1)}}\right)_{\not{V}^{(1)},N^{(1)}} dU^{(1)} + \left(\frac{\partial S^{(1)}}{\partial \not{V}^{(1)}}\right)_{U^{(1)},N^{(1)}} d\not{V}^{(1)} + \\ &\left(\frac{\partial S^{(2)}}{\partial U^{(2)}}\right)_{\not{V}^{(2)},N^{(2)}} dU^{(2)} + \left(\frac{\partial S^{(2)}}{\partial \not{V}^{(2)}}\right)_{U^{(2)},N^{(2)}} d\not{V}^{(2)} \end{aligned} \tag{3.63}$$

Taking into consideration that this is a closed system and that energy/volume gain for one subsys-

tem is equivalent to energy/volume loss of the other. Mathematically

$$dU^{(2)} = -dU^{(1)} \tag{3.64}$$

and

$$d\cancel{V}^{(2)} = -d\cancel{V}^{(1)} \tag{3.65}$$

furthermore, from classical thermodynamic formulation, note that

$$\begin{aligned} \left(\frac{\partial S}{\partial U}\right)_{\cancel{V},N} &= \quad \frac{1}{T} \text{ , temperature} \\ \left(\frac{\partial U}{\partial \cancel{V}}\right)_{U,N} &= -\, P \text{ , pressure} \end{aligned} \tag{3.66}$$

by eqs. (3.64) to (3.66), eq. (3.63) can now be expressed as

$$dS = \left(\frac{1}{T^{(1)}} - \frac{1}{T^{(2)}}\right) dU^{(1)} + \left(\frac{P^{(1)}}{T^{(1)}} - \frac{P^{(2)}}{T^{(2)}}\right) d\cancel{V}^{(1)} = 0 \tag{3.67}$$

Since eq. (3.67) must vanish for any arbitrary and independent values of $dU^{(1)}$ and $d\cancel{V}^{(1)}$, then the following must be true

$$\frac{1}{T^{(1)}} - \frac{1}{T^{(2)}} = 0 \tag{3.68}$$

and

$$\frac{P^{(1)}}{T^{(1)}} - \frac{P^{(2)}}{T^{(2)}} = 0 \tag{3.69}$$

The results of eqs. (3.68) and (3.69) are the equilibrium conditions of the system in the absence of internal constraints using thermodynamic formulation and reasoning dictating that pressure and temperature of both subsystems must come to equilibrium, hence, indicating the necessity to im-

plement such a mechanism to allow for the flashing of steam to occur if the model is to mimic naturally occurring phenomenon.

To compute the amount of flash steam, $\dot{m}_{L2V}$, we make use of eq. (3.57). For mass transfer to occur from subcooled liquid water ($C\cancel{V}_{liq}$) to vapor ($C\cancel{V}_{vap}$), the following condition must be satisfied

$$P_{liq} = P_{sat}\left(T_{liq}\right) > P_{vap} \longrightarrow \dot{m}_{L2V} > 0 \; and \; \dot{T}_{liq} = 0 \tag{3.70}$$

Enforcing the condition of $\dot{T}_{liq} = 0$ and solving for $\dot{m}_{L2V}$ yields the following expression

$$\dot{m}_{L2V} = \frac{E_{V2L} - E_{out} + E_{other} + \dot{Q}_{Net}}{h_{L2V} - u_{liq}} \tag{3.71}$$

Once again, with E_{V2L} being computed in $C\cancel{V}_{vap}$, E_{out} and E_{other} being known, we can evaluate the expression for the amount of flash steam being generated and transferred into $C\cancel{V}_{vap}$, which in turn allows us to compute the mass of the condensate liquid found in the condenser's hotwell by integrating eq. (3.54)

$$m_{liq}\left(t\right) = \int_{t_0}^{t} \left(\dot{m}_{V2L} - \dot{m}_{L2V} - \dot{m}_{out} + \dot{m}_{other}\right) dt + m_{liq}\left(t = t_0\right) \tag{3.72}$$

With the mass of the condensate liquid determined, the volume of the water found in the hotwell is computed as

$$\cancel{V}_{liq} = \frac{m_{liq}}{\rho_{liq}} \tag{3.73}$$

To maintain the model as dynamic as possible, the liquid density, ρ_{liq}, was computed using a temperature dependent approximation proposed by The American Institute of Chemical Engineers

(AIChE). The Design Institute for Physical Properties (DIPPR) branch of the AIChE proposed the following equation

$$\rho_{liq}(T) = \frac{A}{B^{1+\left(1-\frac{T}{C}\right)^{D}}} \tag{3.74}$$

where $\rho_{liq}(T)$ is the density of liquid water at a given temperature and T is the temperature of the liquid water. Furthermore, A, B, C, and D are constant coefficients with their values being tabulated in table 3.5 [48].

Table 3.5: Density coefficients for eq. (3.74)

	A	**B**	**C**	**D**
Value	0.14395	0.0112	649.727	0.05107

A snapshot of $C\forall_{liq}$ modeled in SPPA-T3000 is shown in fig. 3.11.

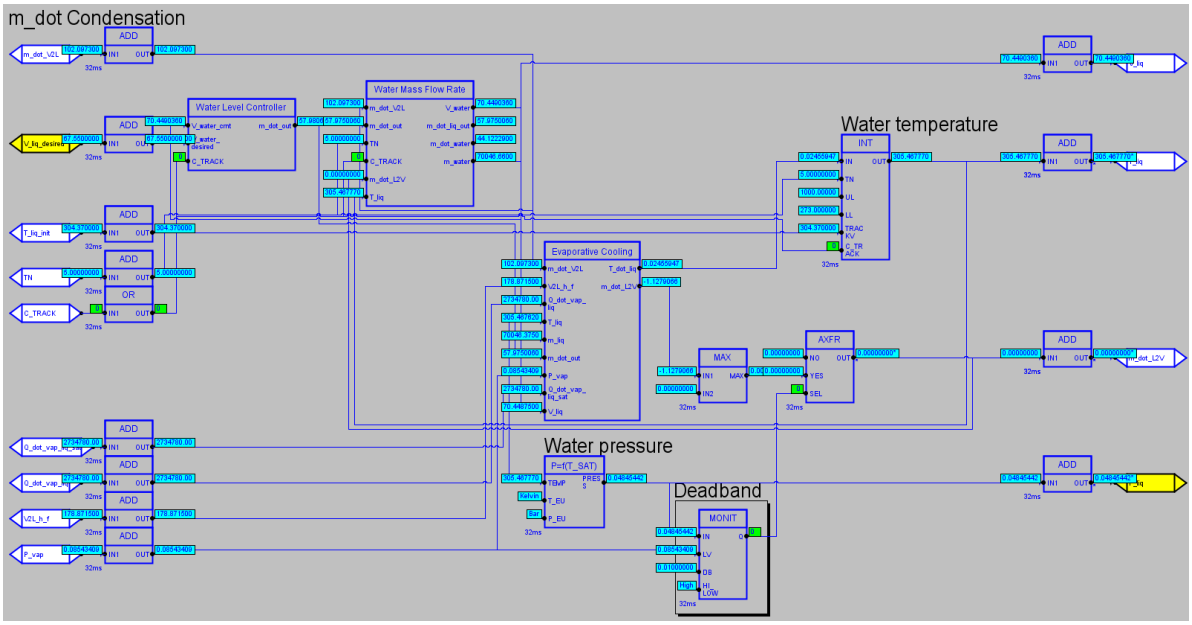

Figure 3.11: Liquid Control Volume ($C\forall_{liq}$) in SPPA-T3000

CHAPTER 4: MODEL VALIDATION

In this chapter, model simulation and validation over a range of cases provided by Siemens Energy Inc. will be examined and compared. Note that Siemens Energy Inc. does not collect transient operation values and as such the model will only be compared against the steady-state values provided. Nonetheless, the model's ability to dynamically adjust and respond to perturbations will be demonstrated by perturbing the system during steady-state operation and allowing it to search for, and settle at, a new equilibrium point corresponding to the new inputs.

In section 4.1, a brief explanation of how the condenser operates from start-up to steady-state operation will be given. In section 4.2, data from multiple different cases provided by Siemens Energy Inc. are compared to the values outputted by the model and a brief discussion will follow. In section 4.4, the model's ability to respond to multiple perturbations will be demonstrated.

4.1 Condenser Operation

The condenser begins operation with the vacuum pump expelling non-condensible gases from within the condenser. Meanwhile, the heat recovery steam generator (HRSG) is generating steam and building pressure until a certain pressure threshold is reached. At that point, a throttle valve used to restrict the mass flow of vapor into the steam turbine for the purposes of building up pressure is slowly opened and steam is allowed to flow into the turbine. The turbine then exhausts the steam into the condenser to be recycled. This throttling valve is out of the scope of this research, nonetheless, a rather simplistic mathematical model of the valve is implemented for the sake of computing the steam approach velocity into the condenser.

Note that the condenser must have already been vacated from all non-condensible gases prior to

the steam being allowed in. While the vacuum pump is ejecting the non-condensibles, the liquid water found in the hotwell experiences a sudden pressure drop on top of it, triggering the flash steam discussed in section 3.3.3 to form. This can be observed in fig. 4.1 at approximately 0.25 minutes ($\approxeq 15\ s$). When the pressure of the liquid water is higher than that of the air above it, flashing occurs, and a build-up of vapor pressure begins.

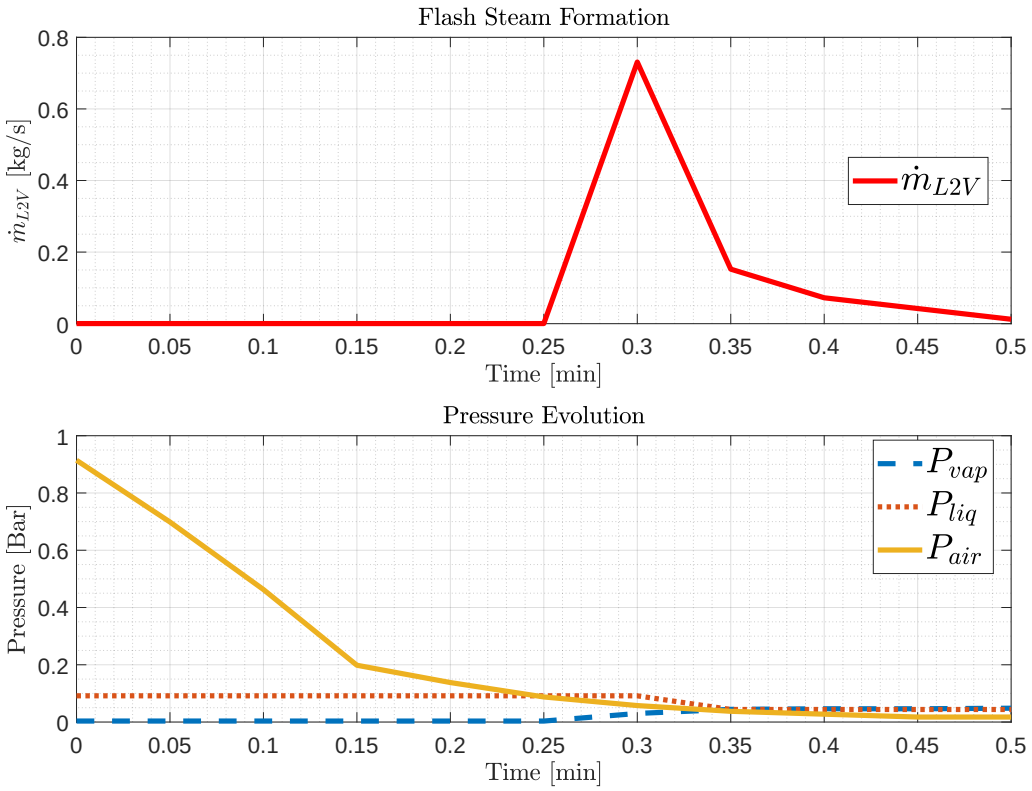

Figure 4.1: Flash steam generation

It must be noted that due to the process at which SPPA-T3000 retrieves data from the archives, a smooth set of points was difficult to obtain and thus the data appears to be discretized and jagged, however, that is not the case when browsing the archived data. This is visible in fig. 4.1, where data points captured do not produce a smooth curve in addition to missing the maximum value of

flash steam achieved as is reported by the archives to be $\max(\dot{m}_{L2V}) = 3.39\ kg\ S^{-1}$ as this mode is short-lived and the exported data did not capture it.

As condensation begins, vacuum conditions within the condenser are induced by the sharp specific volume drop of the condensing vapor, at which point the vacuum pump is running at minimal capacity to ensure that inwards leakage of non-condensibles into the condenser is dealt with.

4.2 Steady-State Values

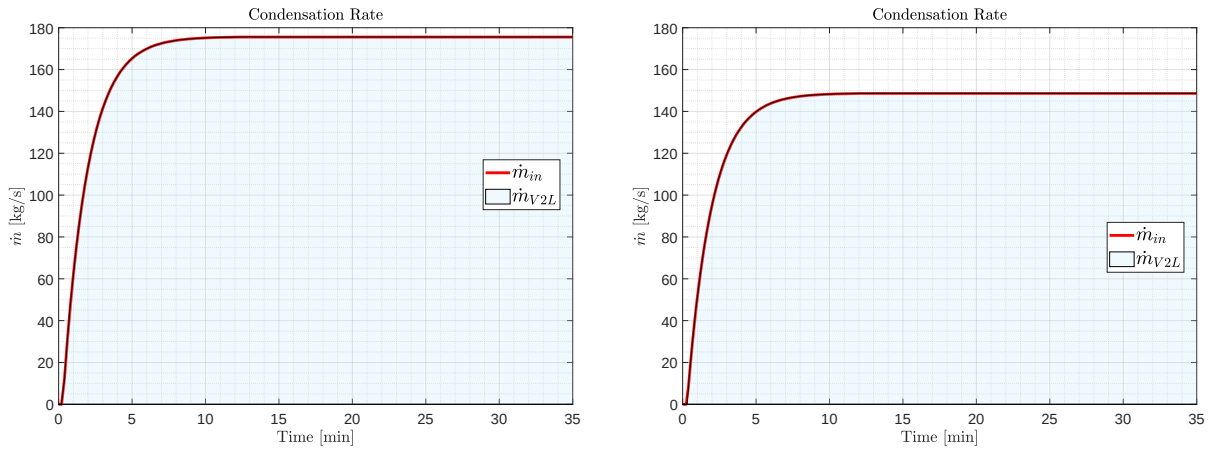

Figure 4.2: Condensation rate. Case 1 (left) and case 2 (right)

In fig. 4.2, the incoming steam from the turbine exhaust is slowly permitted to enter the condenser as is explained in section 4.1. By observing fig. 4.2, the condenser manages to condense all the incoming steam being exhausted from the turbine. At approximately 35 minutes of operation, the system reaches steady-state. The startup of the condenser assumes that the HRSG is already pressurized and ready to send steam through the turbine, as such, the timescale only reflects the time required for the vacuum pump to eject the non-condensible gases out of the condenser and not the time it took the HRSG to pressurize and allow steam into the turbine.

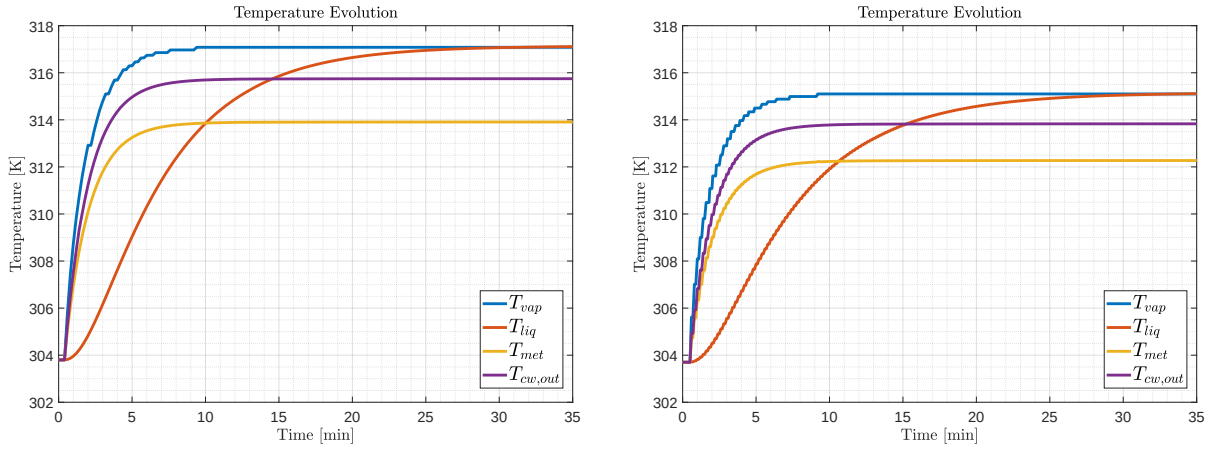

Figure 4.3: Temperature evolution. Case 1 (left) and case 2 (right)

In fig. 4.3, the temperature evolution of the system alongside the switching mechanism described in section 3.2 are both demonstrated. The switching mechanism manifests itself in the figure as the stair-stepping behavior in the vapor temperature, T_{vap}. Once again, it must be noted that due to the process at which SPPA-T3000 retrieves data from the archives, the switching mechanism was not completely captured in the exported data, however, it was clearly visible in the archives and the trend plots generated by SPPA-T3000.

Furthermore, the condensate water, T_{liq}, can be observed to approach the same temperature as that of the vapor at steady state operation, which occurs at about 35 minutes. Note that out of all the dynamics in the model, the condensate liquid's temperature has the lowest response to change as is expected, as liquid water has huge thermal inertia.

Lastly, the pressure evolution of the system can be observed in fig. 4.4. It is evident from the plot that the condenser pressurizes suddenly as soon as flash steam is formed. This transfer of mass from the condensate liquid ($C\cancel{V}_{liq}$) to the vapor space ($C\cancel{V}_{vap}$) causes the liquid water pressure to drop in response.

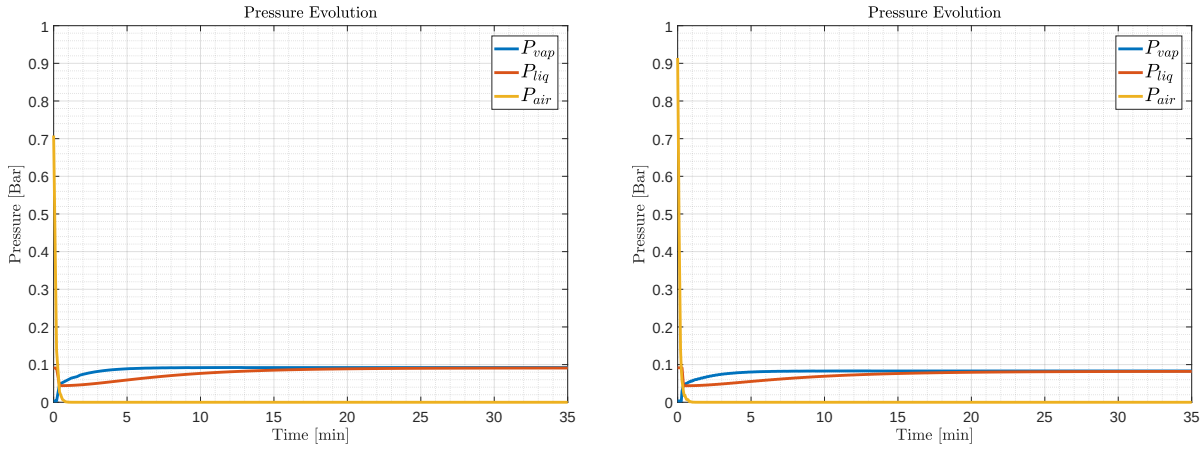

Figure 4.4: Pressure evolution. Case 1 (left) and case 2 (right)

4.3 Simulations

To maintain numerical stability in the simulation, the runtime container has been dilated to five times its value, that is, the model takes a multiplicative factor of five to simulate one clock cycle. For instance, the runtime container was set to run at $32ms$, with the time dilation factor accounted for, it would take the simulation $5 \times 32ms = 0.16s$ to simulate $32ms$ in real-time. The importance of the time dilation factor is most notably viewed when examining Case 6 and Case 7 provided in table 4.1. By examining the model in the SPPA-T3000 GUI while those two cases were being simulated, it was noted that whenever the condenser pressure approached the unusually low pressures tabulated in the data, the system began to slowly oscillate, and said oscillations immediately blew up and the physics of the system was not able to correct for the exponential growth in oscillations, hence, the lack of simulated data values in table 4.1 for both cases. Nonetheless, the oscillations were dealt with by implementing filters that smoothed the data in an attempt to prevent the sudden growth of oscillatory behavior due to the numerical instability, however, the implementation of the filters caused the system's response to deviate from naturally expected behavior, and as such, the

filters were opted out of the model and a viable solution was left for future work.

Ten different operating scenarios with steady-state values were provided by Siemens Energy Inc. that tabulated, among other things, the condenser pressure (P_{vap}), condensate temperature (T_{liq}), coolant inlet temperature ($T_{cw,in}$), coolant exit temperature ($T_{cw,in}$), and condenser heat duty ($\dot{Q}_{HX}$).

Table 4.1: Comparison of model output vs. Siemens' data at steady-state operation

Parameter	**Units**	**Case 1**		**Case 2**		**Case 3**		**Case 4**		**Case 5**	
		Data	Model	Data	Model	Data	Model	Data	Model	Data	Model
Condenser Pressure	Bar	0.09266	0.09220	0.08494	0.08502	0.08287	0.08312	0.07887	0.07876	0.07481	0.07536
Condensate Temperature	K	317.48	317.08	315.76	315.56	315.32	315.10	314.37	314.13	313.37	313.29
Coolant Inlet Temperature	K	303.80	303.80	303.70	303.70	303.70	303.70	303.50	303.50	303.50	303.50
Coolant Exit Temperature	K	315.20	315.75	313.80	314.23	313.30	313.83	312.50	312.86	311.70	312.04
Condenser Heat Duty	$MWth$	396.60	414.40	351.10	372.20	338.40	357.20	313.00	330.30	286.40	301.00

Parameter	**Units**	**Case 6**		**Case 7**		**Case 8**		**Case 9**		**Case 10**	
		Data	Model	Data	Model	Data	Model	Data	Model	Data	Model
Condenser Pressure	Bar	0.03585	–	0.03447	–	0.07412	0.07541	0.06564	0.06604	0.06398	0.06311
Condensate Temperature	K	300.21	–	299.54	–	313.21	313.03	310.93	309.56	310.48	309.97
Coolant Inlet Temperature	K	285.90	285.90	285.90	285.90	298.80	298.80	298.50	298.50	298.40	298.40
Coolant Exit Temperature	K	296.90	–	293.90	–	310.70	311.39	308.70	309.32	308.30	308.84
Condenser Heat Duty	$MWth$	382.70	–	279.90	–	413.90	441.80	356.70	382.10	345.00	367.30

4.4 Response to Perturbation

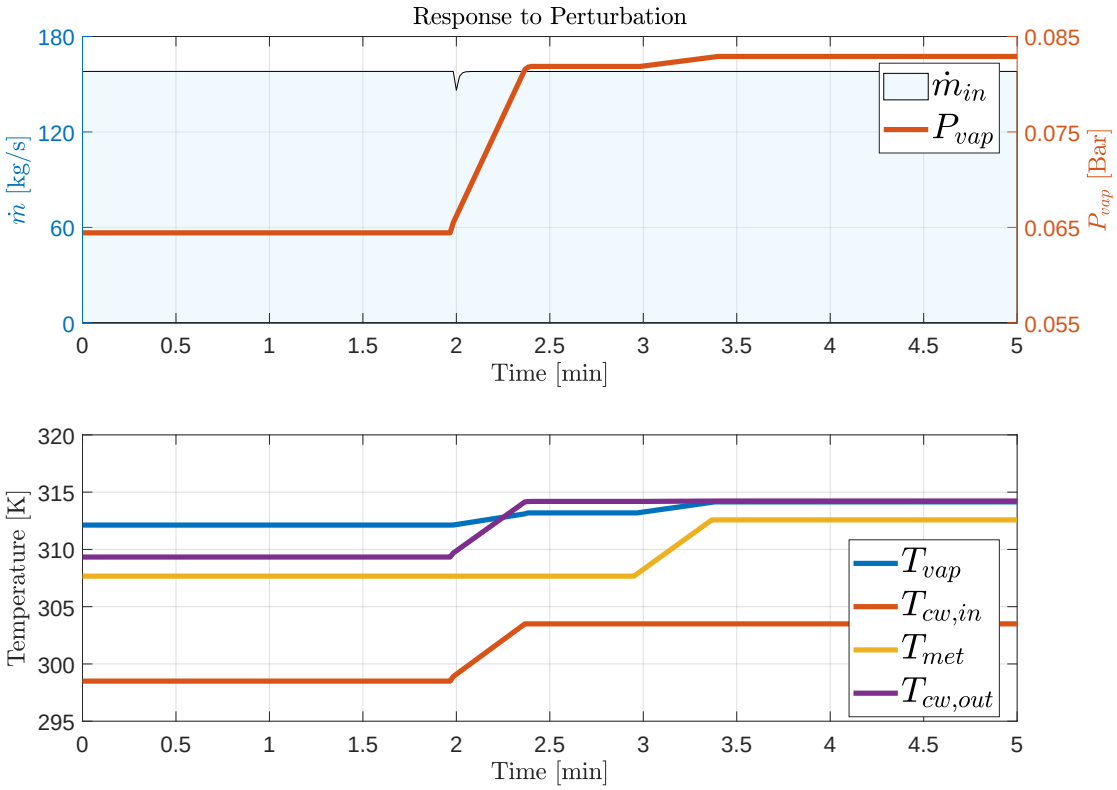

Figure 4.5: Dynamic response

Due to the lack of transient data for model validation purposes, a simple test to measure the model's ability to respond to perturbations in a manner consistent with acceptable thermodynamic behavior was used. To demonstrate that, the model was run and allowed to reach steady-state operation. Once the model was operating at steady-state, the control on the steam valve discussed in section 4.1 was disabled and maintained at fully open position as it acts as a failsafe, causing the model to trip in case of a sudden increase in pressure, the model was then subjected to a perturbation in the form of a five degrees change in temperature at the coolant inlet at time $t = \tau$, that

is,

$$\begin{aligned} T_{cw,in}(t < \tau) &= 298.5K \\ T_{cw,in}(t \geq \tau) &= 303.5K \end{aligned} \tag{4.1}$$

However, to better mimic natural phenomenon, the perturbation was not in the form of a step input, but rather a quick ramp, simulating the scenario where a fan array in the cooling tower might have malfunctioned.

As observed in fig. 4.5, once the perturbation was introduced, the condensation rate, depicted by the flooded area, experiences a sudden decrease as the system begins to adjust its equilibrium position. This sudden drop in condensation rate caused the system to pressurize, triggering the third mode of heat and mass transfer discussed in section 3.2.4 and expressed mathematically in eq. (3.45) as the saturation temperature at the resulting pressure is higher than that of the vapor space. Notwithstanding, it must be noted that any further increase in the cooling water inlet temperature would have caused the system to experience a severe drop in condensation rates, causing a huge rise in pressure within the condenser, and during normal operation where the controls on the steam valve are fully functional the system would have tripped and diverted steam.

CHAPTER 5: CONCLUSION AND FUTURE WORK

5.1 Overview

A mathematical model of Combined Cycle Power Plant (CCPP) condenser has been developed using first principle formulation and a lumped control volume approach. The model was able to accurately predict performance and showed good agreement with the steady-state values provided by Siemens Energy Inc. in addition to showing good response to perturbation consistent with acceptable thermodynamic behavior.

Moreover, the incorporation of empirically and analytical formulations to accurately compute time-varying derived thermodynamic quantities and other heat transfer and fluid flow related coefficients ensured the simulation's validity over a wide range of operating conditions and allowed the model to better predict condensation rates. Likewise, these formulations assisted the model in predicting and simulating the different modes of heat and mass transfer associated with condenser operation, such as the phase change from steam to liquid water and liquid water to steam, where the latter occurs over very short periods of time and is required for thermodynamic stability. The combination of all three modes, namely cooling, condensation, and heating, required the implementation of a switching logic that transitions between all different modes seamlessly such that the model can accurately represent the process of temperature change and mass transfer associated with each mode. The implementation of the switching logic presented in section 3.2.4 proved to be effective in capturing all modes required for heat and mass transfer and was once again able to predict the formation of condensate and the generation of flash steam, when appropriate.

5.2 Future Research

While the research presented in this paper meets the required objective of modeling and simulating a CCPP condenser, further improvements and developments can still be achieved.

5.2.1 Improvements

As was observed in section 4.2, cases 6 and 7 failed to simulate and became immediately unstable due to the unusually low operating pressures encountered within the condenser. Much of the future work would focus on pinpointing the root cause of the oscillations and debugging the implementation of the mathematical formulation in such a manner that is still consistent with thermodynamic principles, as the model is required to be able to operate under all thermodynamically permissible conditions regardless of operating conditions, such as low pressure conditions in both cases.

5.2.2 Superheated Steam HTC Prediction

While the model incorporated a time-varying HTC calculation during the condensation process based on the original work presented by Nusselt, it did not provide a formulation to compute a time-varying HTC for steam that is above saturation conditions.

Based on empirical data provided by Spirax Sarco [49], a steam processes engineering company, superheated steam has a much lower HTC than saturated steam and is usually 10% of the HTC for saturated steam, that is, $H_{sh} = 0.1H_{sat}$. Further research can be done in order to accurately compute and calculate time-varying values for the HTC during cooling mode.

5.2.3 Attemperation

Further research could also be geared towards the process of steam attemperation, which is a process in which superheated steam is brought down to around saturation conditions prior to being allowed into the condenser. Steam attemperation takes place during bypass cases where the steam from the HRSG is not passed to the steam turbine for expansion and power extraction but rather bypassed and sent directly into the condenser. Upstream of the condenser's inlet exist an array of spray nozzles that inject the superheated steam with atomized cooling water, causing the superheated steam to transfer some of its energy into the atomized water and vaporizing it in the process while bringing the level of superheat down to within $3°C$ of the saturation temperature.

While the logic for steam attemperation was developed and an embedded function diagram was prepared, the implementation and testing was not a high priority at the time of writing this thesis, as most operational cases required the steam to be at saturation conditions prior to entering the condenser. Rigorous validation of the attemperation logic and embedded function diagram is left as future research.

5.2.4 Implementation with HRSG, Steam Turbine, and Pump Models

While the mathematical model of the condenser presented within this research provides accurate predictions to condenser performance, implementing this model in conjunction with a HRSG model such as the one developed by McConnell [50], a steam turbine model, and a condensate pump would complete the process described by the Rankine cycle and allow for a better insight and a more accurate representation of the system and its ability to respond to perturbations upstream and downstream of the condenser.

APPENDIX : SPPA-T3000 MODEL

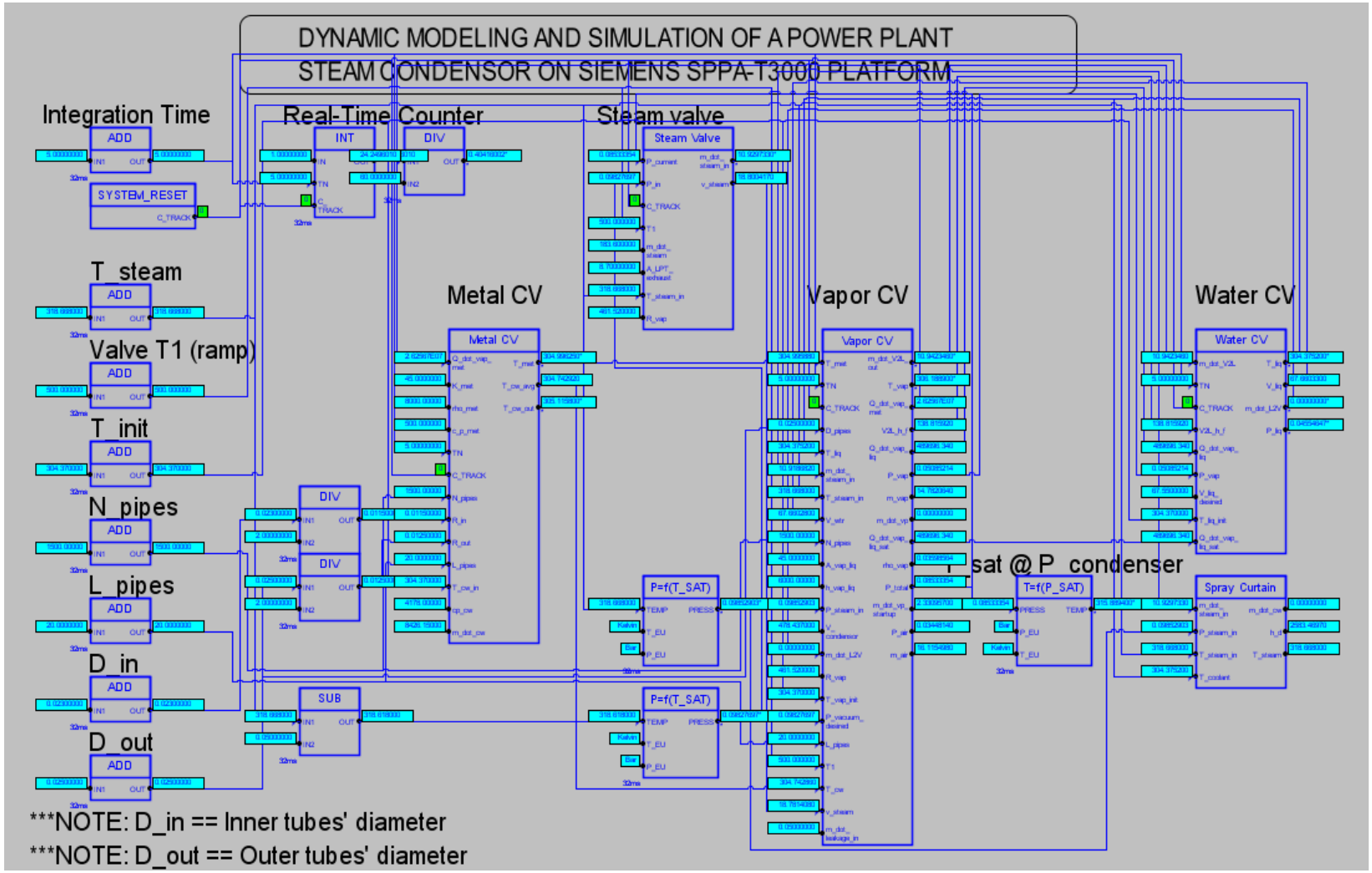

Figure .1: Model in SPPA-T3000

LIST OF REFERENCES

[1] Hausfather, Z., Drake, H. F., Abbott, T., and Schmidt, G. A. "Evaluating the performance of past climate model projections". *Geophysical Research Letters*.

[2] Great Barrier Reef Marine Park Authority, 2014. "Great barrier reef outlook report 2014".

[3] O'Donnell, A. J., Boer, M. M., McCaw, W. L., and Grierson, P. F., 2011. "Climatic anomalies drive wildfire occurrence and extent in semi-arid shrublands and woodlands of southwest australia". *Ecosphere,* **2**(11), pp. 1–15.

[4] Zemp, M., Frey, H., Gärtner-Roer, I., Nussbaumer, S. U., Hoelzle, M., Paul, F., Haeberli, W., Denzinger, F., Ahlstrøm, A. P., Anderson, B., et al., 2015. "Historically unprecedented global glacier decline in the early 21st century". *Journal of Glaciology,* **61**(228), pp. 745–762.

[5] Tahri, T., Abdul-Wahab, S., Bettahar, A., Douani, M., Al-Hinai, H., and Al-Mulla, Y., 2009. "Simulation of the condenser of the seawater greenhouse: Part i: Theoretical development". *Journal of thermal analysis and calorimetry,* **96**(1), pp. 35–42.

[6] Aminov, Z., Nakagoshi, N., Xuan, T. D., Higashi, O., and Alikulov, K., 2016. "Evaluation of the energy efficiency of combined cycle gas turbine. case study of tashkent thermal power plant, uzbekistan". *Applied Thermal Engineering,* **103**, pp. 501–509.

[7] Kakac, S., Liu, H., and Pramuanjaroenkij, A., 2002. *Heat exchangers: selection, rating, and thermal design*. CRC press.

[8] Halle, H., Chenoweth, J., and Wambsganss, M., 1988. "Shellside waterflow pressure drop distribution measurements in an industrial-sized test heat exchanger".

[9] Zhang, C., 1994. "Numerical modeling using a quasi-three-dimensional procedure for large power plant condensers".

[10] Roy, R., Ratisher, M., and Gokhale, V., 2000. "A computational model of a power plant steam condenser". *J. Energy Resour. Technol.,* **123**(1), pp. 81–91.

[11] Cao, Y., 2008. "Dynamic modelling of a steam condenser". *available online[access on 23rd July 2017] http://read. pudn. com/downloads146/doc/635408/steam% 20condenser/dynamic% 20condenser% 20model. pdf.*

[12] Bourdouxhe, J.-P. H., Grodent, M., Silva, K., Lebrun, J., and Saavedra, C., 1994. A toolkit for primary hvac system energy calculation. part 2: reciprocating chiller models. Tech. rep., American Society of Heating, Refrigerating and Air-Conditioning Engineers.

[13] Nikitin, K., Kato, Y., and Ishizuka, T., 2008. "Steam condensing–liquid co2 boiling heat transfer in a steam condenser for a new heat recovery system". *International journal of heat and mass transfer,* **51**(17-18), pp. 4544–4550.

[14] Llopis, R., Cabello, R., and Torrella, E., 2008. "A dynamic model of a shell-and-tube condenser operating in a vapour compression refrigeration plant". *International journal of thermal sciences,* **47**(7), pp. 926–934.

[15] Cuevas, C., Lebrun, J., Lemort, V., and Ngendakumana, P., 2009. "Development and validation of a condenser three zones model". *Applied Thermal Engineering,* **29**(17-18), pp. 3542–3551.

[16] Vanek, F., Albright, L., and Angenent, L., 2008. *Energy systems engineering*. McGraw-Hill Professional Publishing.

[17] Rankine Cycle – Steam Turbine Cycle. `https://www.nuclear-power.net/nuclear-engineering/thermodynamics/thermodynamic-cycles/rankine-cycle-steam-turbine-cycle/`. (Accessed on 02/03/2020).

[18] SPPA-T3000 control system. https://new.siemens.com/global/en/products/automation/distributed-control-system/sppa-t3000.html. (Accessed on 01/31/2020).

[19] Caesar, A., 2018. "Thermodynamic modeling and transient simulation of a low-pressure heat recovery steam generator using siemens T3000".

[20] Kakaç, S., 1991. *Boilers, evaporators, and condensers*. John Wiley & Sons.

[21] Buecker, B., 2002. *Basics of boiler and HRSG design*. Pennwell Books.

[22] Carey, V. P., 2018. *Liquid vapor phase change phenomena: an introduction to the thermophysics of vaporization and condensation processes in heat transfer equipment*. CRC Press.

[23] Butterworth, D., 1977. "Developments in the design of shell and tube condensers". *ASME paper,* **77**.

[24] Shekriladze, I. G., and Gomelauri, V., 1966. "Theoretical study of laminar film condensation of flowing vapour". *International Journal of Heat and Mass Transfer,* **9**(6), pp. 581–591.

[25] Nusselt, W., 1916. "The condensation of steam on cooled surfaces". *Z. Ver. Dtsch. Ing,* **60**, pp. 541–546.

[26] Ddbst - ddbst gmbh. http://www.ddbst.com/. (Accessed on 02/12/2020).

[27] Kays, W. M., 2012. *Convective heat and mass transfer*. Tata McGraw-Hill Education.

[28] Rose, J., 1988. "Fundamentals of condensation heat transfer: laminar film condensation". *JSME international journal. Ser. 2, Fluids engineering, heat transfer, power, combustion, thermophysical properties,* **31**(3), pp. 357–375.

[29] Mandelzweig, S., 1961. "The effect of vertically downward velocity on the heat transfer from a steam-nitrogen mixture condensing on a horizontal cylinder". PhD thesis, University of London (Queen Mary College).

[30] Gogonin, I., and Dorokhov, A., 1971. "Heat transfer from condensing freon-21 vapour moving over a horizontal tube". *Heat Transfer-Soviet Research,* **3**, pp. 157–161.

[31] Tetsu, F., Haruo, U., and Chikatoshi, K., 1972. "Laminar filmwise condensation of flowing vapour on a horizontal cylinder". *International Journal of Heat and Mass Transfer,* **15**(2), pp. 235–246.

[32] Nobbs, D., and Mayhew, Y., 1976. "Effect of downward vapour velocity and inundation on condensation rates on horizontal tube banks". In Symp. on Steam Turbine Condensers, pp. 39–52.

[33] Gogonin, I., and Dorokhov, A., 1976. "Experimental investigation of heat transfer with the condensation of the moving vapor of freon-21 on horizontal cylinders". *Journal of Applied Mechanics and Technical Physics,* **17**(2), pp. 252–257.

[34] Fujii, T., Honda, H., and Oda, K., 1979. "Condensation of steam on a horizontal tube—the influence of oncoming velocity and thermal condition at the tube wall". *Condensation Heat Transfer*, pp. 35–43.

[35] Lee, W., and Rose, J. W., 1982. "Film condensation on a horizontal tube-effect of vapour velocity". In International Heat Transfer Conference Digital Library, Begel House Inc.

[36] Lee, W. C., 1982. "Filmwise condensation on a horizontal tube in the presence of forced convection and non-condensing gas". PhD thesis.

[37] Honda, H., Nozu, S., and Fujii, T., 1982. "Vapour to coolant heat transfer during condensation of flowing vapour on a horizontal tube". In International Heat Transfer Conference Digital Library, Begel House Inc.

[38] Lee, W., Rahbar, S., and Rose, J., 1983. Forced convection film condensation of refrigerant-113 and ethanediol on a horizontal tube. Tech. rep., GEC Energy Systems Ltd., Leicester.

[39] Memory, S., and Rose, J. W., 1986. "Film condensation of ethylene glycol on a horizontal tube at high vapour velocity". In International Heat Transfer Conference Digital Library, Begel House Inc.

[40] Michael, A., Daniels, L., and Rose, J., 1987. *Heat-transfer measurements during condensation of high velocity steam on a horizontal tube*. UKAEA Atomic Energy Research Establishment Thermal Hydraulics Division.

[41] Hewitt, G. F., Shires, G. L., and Bott, T. R., 1994. *Process heat transfer*, Vol. 113. CRC press Boca Raton, FL.

[42] Vestfálová, M., and Šafařík, P., 2016. "Dependence of the isobaric specific heat capacity of water vapor on the pressure and temperature". In EPJ Web of Conferences, Vol. 114, EDP Sciences, p. 02133.

[43] Çengel, Y. A., and Boles, M. A., 2019. Thermodynamics: an engineering approach, 9th edition.

[44] Research, A., on Water, T. C., and in Thermal Power Systems. Water Technology Subcommittee, S., 2002. *Consensus for the lay-up of boilers, turbines, turbine condensers, and auxiliary equipment: an ASME research report*, Vol. 66. American Society of Mechanical Engineers.

[45] Cycling, S., 1998. "Shutdown, and layup—fossil plant cycle chemistry guidelines for operators and chemists". *Electric Power Research Institute, Palo Alto, CA, August*, pp. 137–147.

[46] e.V., V. P., 2009. Guideline for the preservation of power plant systems, vgb-r 116 e. https://www.vgb.org/vgbmultimedia/VGB_M+116+e+Content-p-3624.pdf. (Accessed on 02/21/2020).

[47] Callen, H. B., 1985. *Thermodynamics and an Introduction to Thermostatistics*. Wiley.

[48] Liquid density calculation by dippr105 equation (water). http://ddbonline.ddbst.de/DIPPR105DensityCalculation/DIPPR105CalculationCGI.exe?component=Water. (Accessed on 03/03/2020).

[49] Superheated steam — spirax sarco. https://www.spiraxsarco.com/learn-about-steam/steam-engineering-principles-and-heat-transfer/superheated-steam. (Accessed on 03/12/2020).

[50] McConnell, J., 2019. "Modeling and transient simulation of a fully integrated multi-pressure heat recovery steam generator using siemens t3000".